Mezger T, Cantow HJ (1984) Cellulose-containing triblock copolymers—syntheses via cellulosic dithiodiaryl photoinitiators. Polym Photochem 5:49–56

Murty KVSN, Xie T, Bernet B, Vasella A (2006) Oligosaccharide analogues of polysaccharides—part 26—mimics of cellulose I and cellulose II: Di- and monoalkynyl c-cellosides of 1, 8-disubstituted anthraquinones. Helv Chim Acta 89:675–730

Nakatsubo F, Maeda K, Murakami K (1987) Reactivity of the reducing-end of cellulose. 1. Preparation of phenylcelluloside. Bull Kyoto Univ Forests 59:301

Ohno K, Koh K, Tsujii Y, Fukuda T (2002) Synthesis of gold nanoparticles coated with well-defined, high-density polymer brushes by surface-initiated living radical polymerization. Macromolecules 35:8989–8993

Pinto RJB, Marques P, Martins MA, Neto CP, Trindade T (2007) Electrostatic assembly and growth of gold nanoparticles in cellulosic fibres. J Colloid Interf Sci 312: 506–512

Pohjola L, Eklund V (1977) Polyurethane block copolymers from cellulose triacetate. Paperi Ja Puu-Paper And Timber 59:117–120

Roche EJ, Obrien JP, Allen SR (1986) Preparation of cellulose triacetate: From solution. Polym Commun 27:138–140

Sata H, Murayama M, Shimamoto S (2004) Properties and applications of cellulose triacetate film. Macromol Symp 208:323–333

Schubert MM, Hackenberg S, van Veen AC, Muhler M, Plzak V, Behm RJ (2001) Co oxidation over supported gold catalysts-"inert" and "active" support materials and their role for the oxygen supply during reaction. J Catal 197: 113–122

Shin Y, Bae IT, Arey BW, Exarhos GJ (2008) Facile stabilization of gold-silver alloy nanoparticles on cellulose nanocrystal. J Phys Chem C 112:4844–4848

Sipahi-Saglam E, Gelbrich M, Gruber E (2003) Topochemically modified cellulose. Cellulose 10:237–250

Sprague BS, Riley JL, Noether HD (1958) Factors influencing the crystal structure of cellulose triacetate. Text Res J 28:275–287

Stannett VT, Williams JL (1976) Modification of wool and cellulose fibers by grafting. J Macromol Sci-Chem A 10:637–652

Steinmann HW (1970) Elastomeric fibers from cellulose triacetate. Polym prepr Am Chem Soc. Div Polym Chem 11:285–290

Stipanovic AJ, Sarko A (1978) Molecular and crystal-structure of cellulose triacetate: - parallel chain structure. Polymer 19:3–8

Strong L, Whitesides GM (1988) Structures of self-assembled monolayer films of organosulfur compounds adsorbed on gold single-crystals—electron-diffraction studies. Langmuir 4:546–558

Sugiyama J, Vuong R, Chanzy H (1991) Electron-diffraction study on the 2 crystalline phases occurring in native cellulose from an algal cell-wall. Macromolecules 24: 4168–4175

Wenz G, Liepold P, Bordeanu N (2004) Monolayers of reactive cellulose derivatives. Macromol Symp 210:203–208

Wenz G, Liepold P, Bordeanu N (2005) Synthesis and sam formation of water soluble functional carboxymethylcelluloses: Thiostilfates and thioethers. Cellulose 12:85–96

Woodcock C, Sarko A (1980) Packing analysis of carbohydrates and polysaccharides.11. Molecular and crystal-structure of native ramie cellulose. Macromolecules 13:1183–1187

Wuelfing WP, Gross SM, Miles DT, Murray RW (1998) Nanometer gold clusters protected by surface-bound monolayers of thiolated poly(ethylene glycol) polymer electrolyte. J Am Chem Soc 120:12696–12697

Yagi S, Kasuya N, Fukuda K (2010) Synthesis and characterization of cellulose-b-polystyrene. Polymer Journal 42:342–348

Yokota S, Kitaoka T, Opietnik M, Rosenau T, Wariishi H (2008) Synthesis of gold nanoparticles for in situ conjugation with structural carbohydrates. Angew Chem Int Ed 47:9866–9869

Yonezawa T, Onoue S, Kimizuka N (2001a) Formation of uniform fluorinated gold nanoparticles and their highly ordered hexagonally packed monolayer. Langmuir 17: 2291–2293

Yonezawa T, Yasui K, Kimizuka N (2001b) Controlled formation of smaller gold nanoparticles by the use of four-chained disulfide stabilizer. Langmuir 17:271–273

J. Japan. Soc. Hort. Sci. 79 (3): 275–281. 2010.
Available online at www.jstage.jst.go.jp/browse/jjshs1

Condensed Tannin Composition Analysis in Persimmon (*Diospyros kaki* Thunb.) Fruit by Acid Catalysis in the Presence of Excess Phloroglucinol

Takashi Akagi, Yasuhiko Suzuki, Ayako Ikegami, Hiroshi Kamitakahara, Toshiyuki Takano, Fumiaki Nakatsubo and Keizo Yonemori***

Graduate School of Agriculture, Kyoto University, Sakyo-ku, Kyoto 606-8502, Japan

Persimmon (*Diospyros kaki* Thunb.) accumulates soluble condensed tannin (CT) in fruit which is responsible for its astringency trait. In this study, we analyzed the CT composition in persimmon fruit with phloroglucinol, and identified and characterized novel epigallocatechin-3-*O*-gallate-phloroglucinol (EGCG-P) adducts as one of the main CT components of persimmon fruit. Analysis with phloroglucinol in persimmon cultivars revealed the different tendencies of the CT composition and component ratio among the four astringency types (PCNA, PVNA, PVA, and PCA), which are categorized by their patterns of astringency loss. The concentration of the main CT component in persimmon fruit, epigallocatechin-3-*O*-gallate (EGCG), was particularly different among astringency types. Further analysis of the fruit at various maturation stages will help in understanding the different mechanisms of CT accumulation among astringent types. Our results demonstrated that the phloroglucinol methodology is useful for CT composition analysis in persimmon fruit and will contribute to future studies on the astringency trait in this fruit.

Key Words: condensed tannin, *Diospyros kaki*, epigallocatechin-3-*O*-gallate, phloroglucinol.

Introduction

Condensed tannin (CT) (also called proanthocyanidin) is a phenolic oligomer resulting from the polymerization of flavan-3-ol units, which consists of two types of subunits, extension and terminal units (Fig. 1A, Aron and Kennedy, 2008; Dixon et al., 2005) and is synthesized via the flavonoid pathway (Dixon et al., 2005; Lepiniec et al., 2006). Flavonoids generally provide protective functions in plants, particularly against herbivores and UV irradiation (McMahon et al., 2000; Winkel-Shirley, 2001). They also act as antioxidants with beneficial effects on human health, including protection against free radicals, and cardiovascular and metabolic diseases (Aron and Kennedy, 2008; Cos et al., 2004). As a final product of the flavonoid pathway, CT also contributes to the quality of many important plant products, such as wine, tea, cocoa and some berries (Aron and Kennedy, 2008).

Japanese persimmon (*Diospyros kaki* Thunb.) accumulates soluble CT in fruit, which is responsible for its strong astringency trait, during the early stages of fruit development. Matsuo and Ito (1978) analyzed the toluene-α-thiol degradation products of persimmon fruit CTs isolated from 'Hiratanenashi' (pollination variant astringency; PVA type). The results suggested that the proposed CT structure consists of two types of flavan-3-ols; catechin (C) and gallocatechin (GC), and their gallate forms; CA-3-*O*-gallate (CG) and GC-3-*O*-gallate (GCG), with a molar ratio of 1 : 2 : 1 : 2, respectively. These units are linked by the C-4 position through C-8; however, this characterization does not refer to the 2,3-cis/trans configuration of flavan-3-ols in persimmon fruit (Fig. 1A, catechin vs. epicatechin and gallocatechin vs. epigallocatechin). The study by Tanaka et al. (1994) is the only study that distinguished this cis/trans configuration of flavan-3-ols by HPLC analysis following thiolysis. This situation is mainly due to technical difficulties in CT composition analysis.

Acid-catalyzed cleavage with benzyl mercaptan or phloroglucinol has been the major method of CT composition analysis (Fig. 1B for methodology, Scofield et al., 2001). Although previous reports suggested that benzyl mercaptan is the preferred reagent, an unpleasant odor that occurs during thiolysis makes it difficult to use

Received; November 5, 2009. Accepted; March 18, 2010.
* Corresponding author (E-mail: keizo@kais.kyoto-u.ac.jp).
** Present address: Laboratory of Pomology, Department of Bioproduction Sciences, Ishikawa Prefectural University, Nonoichi 921-8836, Japan.

(Scofield et al., 2001). However, the problem of low efficiency in the reaction with phloroglucinol has been reported by Scofield et al. (2001). A recent study by Kennedy and Jones (2001) clearly justified the use of excess phloroglucinol in acid-catalyzed cleavage studies of CT in grapevine (*Vitis vinifera*). CT composition analyses in apple (*Malus* × *domestica*), *Arabidopsis thaliana* and other plant species using the same method showed that acid-catalyzed cleavage with excess phloroglucinol is a convenient and effective method (Pang et al., 2007; Pourcel et al., 2005; Takos et al., 2006).

In this study, we applied the same method using phloroglucinol to analyze CT composition in persimmon fruit. In preliminary analyses with phloroglucinol, we detected three peaks for flavan-3-ols phloroglucinol ad-

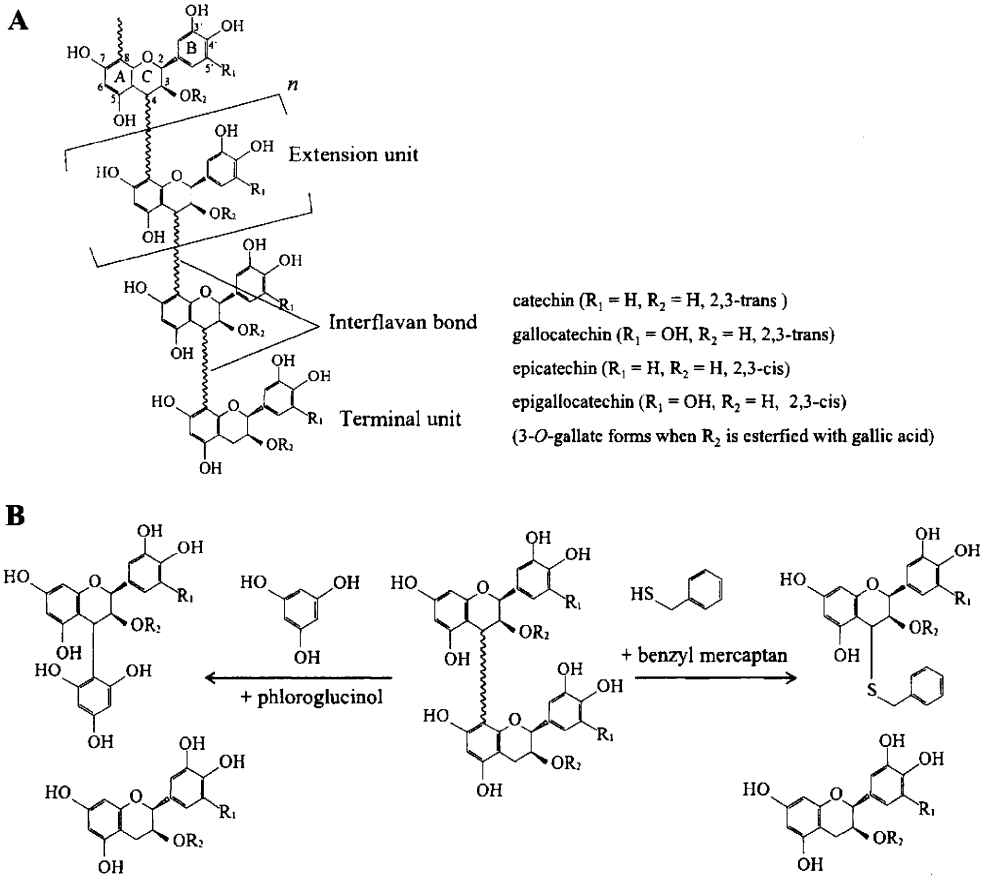

Fig. 1. Representative condensed tannin (CT) structure (A) and methodology for CT composition analysis with phloroglucinol or thiophenol (B). (A) Each CT component is shown with their structure depending on the groups at the 5' position of the B-ring (R_1), 3 position of the C-ring (R_2), and 2,3-cis/trans configuration of the C-ring. (B) When phloroglucinol (left) or thiophenol (right) undergoes nucleophilic addition to the 4 position, we can detect extension units as phloroglucinol or thiophenol adducts, respectively, while terminal units as monomers.

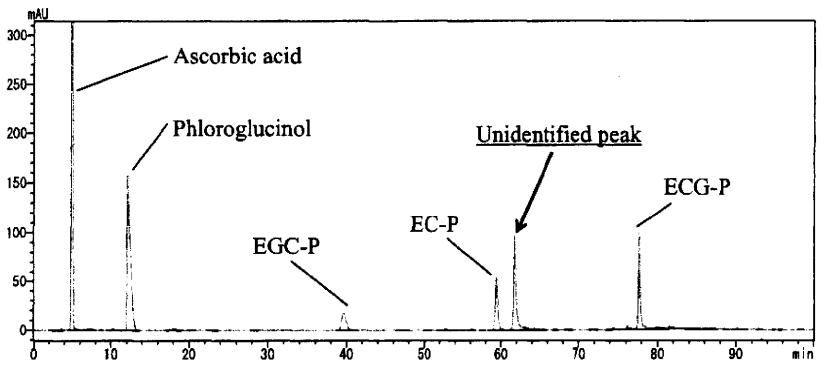

Fig. 2. HPLC profile for 'Yokono' phloroglucinol adduct analysis.

ducts; epicatechin-phloroglucinol (EC-P), epigallocatechin-phloroglucinol (EGC-P) and epicatechin-3-*O*-gallate-phloroglucinol (ECG-P), and one for an unidentified major peak (Fig. 2). Persimmons are classified into four types according to the pattern of astringency-loss on the tree; (i) pollination-constant non-astringent (PCNA), (ii) pollination-variant non-astringent (PVNA), (iii) pollination-variant astringent (PVA) and (iv) pollination-constant astringent (PCA) (Yonemori et al., 2000). We initially tried to identify this uncharacterized major peak by acid catalysis with phloroglucinol and to quantify the phloroglucinol adducts among the four types of persimmon cultivars. We also aimed to reveal the different tendencies of the CT composition and component ratios among these astringency types. Our approaches using phloroglucinol disclosed that the CT composition in persimmon fruit and its analysis may provide new insight into CT polymerization mechanisms, which are now sought in the field of plant science (Xie and Dixon, 2005), because the degree of polymerization in persimmon fruit is considerably higher than that in other plant species (Aron and Kennedy, 2008; Matsuo and Itoo, 1978).

Materials and Methods

Plant materials

Immature 'Yokono' (PCA) fruits were sampled in the experimental orchard of Kyoto University, Kyoto, Japan, on July 2, 2008 to isolate and characterize the unidentified major peak in HPLC analysis with phloroglucinol (Fig. 2). Immature 'Mikado' (PCNA), 'Sangoku-ichi', 'Niikura' (PVNA), 'Akadzu', 'Hiratanenashi' (PVA), 'Yokono', and 'Miyazaki-tanenashi' (PCA) fruits were sampled in the same orchard for CT composition analyses among these astringency types. 'Jiro' (PCNA) fruits were sampled in the Experimental Farm of Kyoto University, Takatsuki, Osaka, Japan. Three fruits per each cultivar were sampled on June 19, 2007. The fruit mesocarp was diced (approximately 0.5 × 0.7 × 1.0 cm) and lyophilized into a freeze-dried sample.

Isolation and characterization of an unidentified major phloroglucinol adduct in persimmon fruit

Freeze-dried (0.995 g) 'Yokono' fruit powder was added directly to 10 mL phloroglucinol reagent (500 mg phloroglucinol and 100 mg ascorbic acid in 1% HCl/MeOH; v/v) and incubated at 50°C for 20 min. This reaction was stopped using 10 mL of 200 mM sodium acetate. After concentrating the aqueous solution, it was extracted with ethyl acetate three times and evaporated under reduced pressure at 35°C. The extract was dissolved in 800 μL MeOH, of which 200 μL was spotted on a reverse-phase thin layer chromatography (TLC) plate and developed with 0.2% aqueous acetic acid to separate the phloroglucinol adducts from excess phloroglucinol. The separated component was collected with TLC, dissolved with 100% MeOH and filtered through a 0.45 μm filter. After concentrating the filtrate under reduced pressure at 35°C, a crude and unidentified component was separated again by TLC developed with toluene : acetone : formic acid (6 : 6 : 1; v/v/v), according to a previous report by Merghem et al. (2004). The isolated component was lyophilized and characterized by ^{1}H-NMR Varian Inova 300 (300 MHz; Varian Inc., Palo Alto, USA), 2D NMR (H-H COSY), and MALDI-TOF MS Bruker Reflux III (Bruker Corporation, Yokohama, Japan) according to the previous report by Zhang and Lin (2008).

The ^{1}H-NMR spectra were recorded on a Varian INOVA 300 spectrometer in acetone-d6/methanol-d4 (1/1, v/v) with tetramethylsilane as an internal standard, by using pulse sequences for one- and two-dimensional spectra. Chemical shifts (δ) and coupling constants (J) are given in δ-values (ppm) and Hz, respectively. MALDI-TOF MS spectra were recorded with Bruker MALDI-TOF MS REFLEX III. For ionization, a nitrogen laser was used. All spectra were measured in the reflector mode using external calibration. Compounds were measured with 2,5-dihydroxybenzoic acid (DHB) as a matrix.

Procedure for determining the CT composition in persimmon fruit

To extract CTs, freeze-dried samples were ground to a fine powder and 10 mg was extracted in 1 mL of 70% acetone with 0.1% ascorbic acid for 24 h in the dark. The samples were then centrifuged, and each of the 200 μL supernatant aliquots were transferred to a new tube and dried under vacuum at 30°C for 60 min. One of the two tubes was used to analyze free monomers of flavan-3-ols and the other was used for acid-catalyzed cleavage of the CT in the presence of excess phloroglucinol by the method mentioned in a previous report by Downey et al. (2003). These reactions were stopped with 200 mM sodium acetate (twice the volume of the phloroglucinol reagent) and then a vanillin solution was added (1 mg vanillin in 5 mL 1% HCl/MeOH; v/v), as the internal standard for subsequent HPLC analysis.

Samples were subjected to reverse-phase HPLC LC2010 (Shimadzu, Tokyo, Japan) using a Wakosil-II 5C18 RS (5 μm, 250 mm × 4.6 mm) analytical column protected by a guard column containing the same material. Elution was performed with 0.2% aqueous acetic acid (solvent A) (v/v) and MeOH (solvent B) using an elution program: 1% B for 30 min, a gradient to 15.5% B for 35 min and gradient to 45% B for 35 min, followed by washing with 100% B for 15 min and a return to the initial conditions (1% B). Analysis was performed at 30°C with a flow rate of 1 mL·min^{-1} and detection at 280 nm. For the LC-MS analysis, we used an LCMS-2010A (Shimadzu) with a Shim-pack VP-ODS (5 μm, 150 mm × 2 mm).

Concentrations of free monomer and hydrolysed terminal subunits were determined by comparing them

with a commercial standard from Sigma-Aldrich (St. Louis, USA). Concentrations of the extension subunit-phloroglucinol adducts were calculated using published molar extinction coefficients (Kennedy and Jones, 2001). The standard curve for the concentration of the unidentified component isolated in the reaction from 'Yokono' fruit powder was newly constructed. Concentrations of all compounds were expressed as (+)-catechin equivalents.

Results and Discussion

Identification of the CT components in persimmon fruit with phloroglucinol

HPLC analysis of five flavan 3-ols and flavan 3-ols gallates phloroglucinol adducts (C-P, EC-P, GC-P, EGC-P, and ECG-P) has been reported in grapevine (Kennedy and Jones, 2001) and pea (Merghem et al., 2004). Based on these reports, we preliminarily analyzed persimmon fruit CTs following acid catalysis in the presence of excess phloroglucinol under the same HPLC conditions but found that some peaks overlapped under these conditions. Hence, we performed the analysis under different conditions (see Materials and Methods) according to the report by Downey et al. (2003), which has been used in other CT studies with phloroglucinol (Bogs et al., 2005; Takos et al., 2006). Using this condition, we detected clearly separated peaks (Fig. 2). HPLC analysis of persimmon ('Yokono'), grapevine ('Delaware') and pea ('Sanren'), and LC/MS analysis of 'Yokono' allowed us to identify EC-P, EGC-P and ECG-P adducts; however, C-P and GC-P adducts were not detected in the persimmon fruit. This result indicates that, except for C and GC the others are contained as extension units of the persimmon fruit CT. Apart from the EC-P, EGC-P, and ECG-P peaks, we detected an unidentified major peak immediately following the EC-P peak (see Fig. 2, indicated by arrow).

As the major peak from 'Yokono' of HPLC, this unidentified major compound was isolated by the TLC method. MALDI-TOF MS analysis of the isolated product using 2,5-dihydroxybenzoic acid (DHB) as a matrix revealed that the molecular weight m/z 605.23 was detected as a pseudo ion peak of sodium adduct. Namely, the molecu-lar weight of the compound is m/z 582. Furthermore, the proton NMR spectrum of the main product revealed that the coupling constant ($J_{2,3}$) of the major compound was approx. 1 Hz, recorded in acetone-d_6/methanol-d_4 (1/1, v/v). The C2 and C3 protons appeared at δ 5.37 (broad s) and 5.25 (dd, J = 1.8 and 1.4 Hz), respectively. On the other hand, Kennedy and Jones (2001) reported that C2 and C3 protons of (−)-epicatechin-3-*O*-gallate-(4β→2)-phloroglucinol appeared at δ 5.45 (d) and 5.23 ppm (dd) with $J_{2,3}$ < 1 Hz, respectively, recorded in acetone-d_6. Davis et al. (1996) reported that C2 and C3 protons of epigallocatechin-3-*O*-gallate appeared at δ 5.07 and 5.56 ppm with $J_{2,3}$ = 1.4 Hz, respectively, recorded in acetone-d_6; however, the coupling constant (J = 6.7 Hz) between H-2 and H-3 of (+)-catechin indicates 2,3-trans configuration (Cai et al., 1991). These studies proved that the main product is epigallocatechin-3-*O*-gallate-(4β→2)-phloroglucinol (EGCG-P) with 2,3-cis configuration. Moreover, the coupling constant (about J = 0 Hz) between H-3 and H4 of epigallocatechin 3-*O*-gallate-

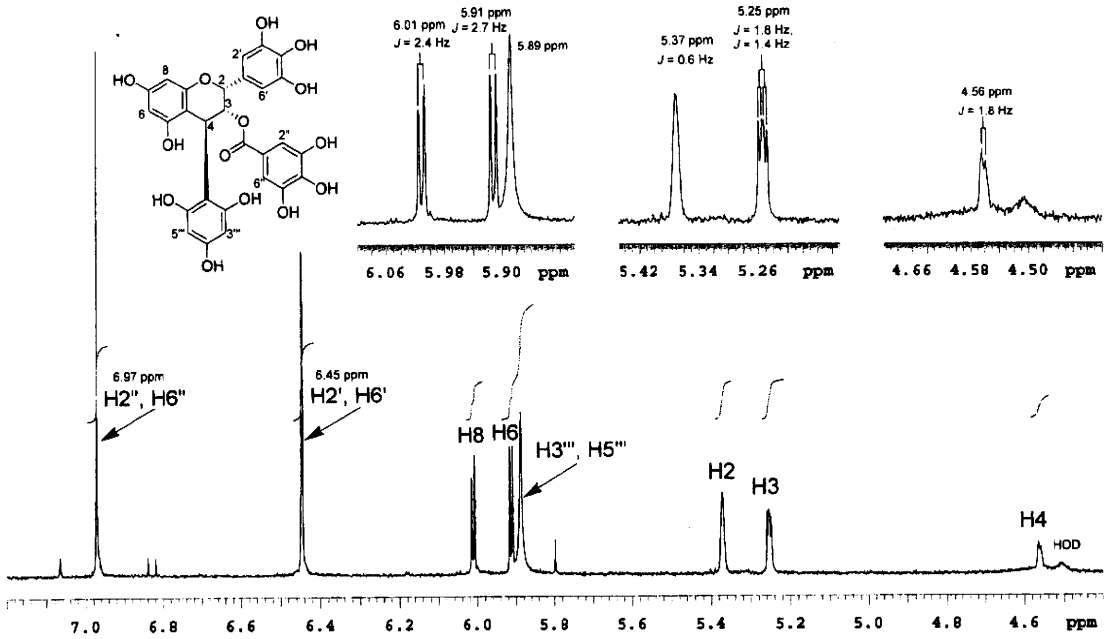

Fig. 3. ^{1}H-NMR spectrum of EGCG-P identified in the 'Yokono' fruit measured in acetone-d_6/methanol-d_4 (1/1, v/v). Proton resonance of HOD at δ 4.51 ppm was decoupled.

(4β→6)-epigallocatechin 3-*O*-gallate indicates 3,4-trans configuration (Hashimoto et al., 1989). Other protons of the main product, C4, C3''' and C5''', C6, C8, C2' and C6', and C2'' and C6'' appeared at δ 4.56 (d, 1H), 5.89 (s, 2H), 5.91 (d, 1H, J=2.7), 6.01 (d, 1H, J=2.4), 6.45 (s, 2H), and 6.97 (s, 2H) ppm, respectively (Fig. 3). Thus, all analytical data indicate that the main product is EGCG-P. We constructed a standard curve for EGCG-P concentration using the following equation: y=0.815x + 116.52 [x; peak area (×1000; AU), and y; EGCG concentration not including the phloroglucinol moiety (μg/10 mg DW)].

Characterization of the CT composition in persimmon cultivars

In phloroglucinol analyses of CTs in persimmon fruit, we mainly detected the formation of phloroglucinol adducts for CT extension units but few hydrolyzed monomers for the terminal CT units were also found (data not shown). This indicates a high degree of CT polymerization in persimmon fruit, which is consistent with a previous report by Matsuo and Ito (1978). We detected four 2,3-cis-flavan 3-ols (i.e. EC, EGC, and their gallate-ester ECG and EGCG) as CT extension units in persimmon fruit (Fig. 2). Anthocyanidin reductase (ANR) and leucoanthocyanidin reductase (LAR) are involved in the biosynthetic pathways of 2,3-cis- and 2,3-trans-flavan 3-ols, respectively (Dixon et al., 2005; Tanner et al., 2003; Xie et al., 2003, 2004). Therefore, the high ratio of 2,3-cis-flavan 3-ols in the persimmon fruit is presumable due to the considerably higher transcript level of *ANR* than that of *LAR*, as suggested in reports by Akagi et al. (2009a, b) and Nakagawa et al. (2008).

On comparing the persimmon cultivars, we could not detect differences in the CT compositions among the four astringency types (P > 0.05), although EGCG concentration was likely lower in the order of PCNA, PVNA, PVA, and PCA cultivars (Table 1). Previous reports suggested that the CT concentration in the PCNA cultivar is markedly reduced after mid-June, whereas non-PCNA cultivars can accumulate CT constantly until August and show little reduction in the concentration of CT (Ikegami et al., 2005). Our results from samples collected on June 19 showed minimal differences in the CT composition and concentration between PCNA and the other three non-PCNA types. Thus, the CT composition in PCNA cultivars may dramatically change accompanied by a change in the CT concentration in later mature stages. In CT component ratio analysis between cultivars, it was indicated that the total ratio of C, EC, and ECG (although CG was not detected), in which the catechol nucleus constitutes the B-ring (see Fig. 1), was clearly higher in PCNA cultivars than that in the other three non-PCNA cultivars (Table 2). These tendencies are consistent with a previous report by Nakatsubo et al. (2002). Concentrations of C, EC, and ECG were slightly high in the PCNA types. Presumably, this was also due to the low EGCG concentration in PCNA, resulting in high C, EC, and ECG ratios against total CT in PCNA cultivars (Table 1). Furthermore, the ratio of the gallate form in the PCNA and PVNA cultivars

Table 1. CT composition in eight persimmon cultivars estimated using phloroglucinol. Each CT component concentration is shown as [mg per 10 mg DW].

	PCNA		PVNA		PVA		PCA	
	'Jiro'	'Mikado'	'Sangokuichi'	'Niikura'	'Hiratanenashi'	'Akadu'	'Yokono'	'Miyazaki-tanenashi'
C	33.1±4.1 b[y,x]	33.9±3.2 b	54.4±5.8 a	39.8±3.2 b	11.1±2.9 d	15.1±1.2 d	22.7±2.2 c	23.6±4.2 bc
GC	12.8±2.9 a	9.8±1.9 a	16.1±2.8 a	6.7±2.8 ab	12.5±4.8 a	1.7±0.8 c	14.3±2.1 a	3.1±1.9 bc
EC	391.7±42.1 a	382.2±41.2 a	362.5±28.8 a	246.3±30.8 b	304.8±32.9 ab	255.9±24.2 b	225.4±17.5 b	271.7±48.2 ab
EGC	706.5±92.4 bc	632.1±109.2 c	1121.0±100.8 a	751.9±82.3 bc	698.3±30.3 bc	734.5±118.1 bc	960.2±90.2 ab	960.0±123.1 ab
ECG	205.8±38.9 bc	321.4±52.3 a	208.7±41.2 bc	151.7±18.8 c	258.2±37.6 ab	218.5±51.2 bc	151.5±22.2 c	203.0±30.9 bc
EGCG	645.8±72.6 cd	902.7±85.1 bc	1392.9±150.4 ab	1176.9±130.7 bc	1532.0±186.1 ab	1626.9±201.2 ab	1754.5±159.6 a	1864.1±214.2 a
total	1982.9 b	2272.3 b	3139.5 a	2366.6 b	2804.4 ab	2851 ab	3114.3 a	3322.4 a

[z] Each component concentration is shown as total amount of extension and terminal units not containing free monomers of flavan 3-ols.
[y] Different letters indicate significant differences among the cultivars at the 5% level (ANOVA followed by Tukey's test).
[x] Extraction and determination of CT components were performed in triplicate. Mean±SD (n=3).

Table 2. Component CT rates (%) that had a galloyl group at the 3 position of the C-ring (gallate form) and whose B-ring contained a catechol.

	PCNA		PVNA		PVA		PCA	
	'Jiro'	'Mikado'	'Sangokuichi'	'Niikura'	'Hiratanenashi'	'Akadu'	'Yokono'	'Miyazaki-tanenashi'
Rate of gallate form CTs	43.7 a[z]	54.7 b	51.9 b	57.1 bc	64.1 d	65.1 d	61.7 cd	62.7 d
Total rate of CTs the catechol constituting the B-ring	30.6 a	31.4 a	18.5 b	17.1 bc	20.2 b	16.7 bc	12.2 d	14.4 d

[z] Different letters indicate significant differences among cultivars at the 5% level (ANOVA followed by Tukey's test).

was lower than that in PVA and PCA cultivars (Table 2), which was also mainly due to differences in EGCG content.

A qualitative difference in the astringency trait between PCNA and the other three non-PCNA types has been suggested (Ikeda et al., 1985). Molecular analysis of CT biosynthesis in PCNA and non-PCNA indicated that the expression levels of many structural genes in the CT biosynthetic pathway show a considerable reduction in PCNA with fruit development (Akagi et al., 2009a, b; Ikegami et al., 2005). Akagi et al. (2009b) also suggested that a reduction in the expression of *DkMyb4*, which is a Myb transcription factor, and the resulting down-regulation of the two structural genes, flavanone 3'5'-hydroxylase (*F3'5'H*) and *ANR*, which are regulated by DkMyb4, are particularly responsible for the differences in the composition or component ratio of the CT in the PCNA type. However, the PVNA, PVA, and PCA types are quantitative traits that are responsible for the quantity of volatile compounds from seeds (Yonemori et al., 2000). It would be interesting to see that different tendencies of the CT composition or component ratio were observed among PVNA, PVA, and PCA in the early mature stages when seeds have not developed (Tables 1 and 2). In this study, we measured the CT composition and component ratio in persimmon cultivars only at one sampling point. More detailed measurements throughout fruit maturation will contribute to characterization of the astringency trait in persimmon fruit.

Literature Cited

Akagi, T., A. Ikegami, Y. Suzuki, J. Yoshida, M. Yamada, A. Sato and K. Yonemori. 2009a. Expression balances of structural genes in shikimate and flavonoid biosynthesis cause a difference in proanthocyanidin accumulation in persimmon (*Diospyros kaki* Thunb.) fruit. Planta 230: 899–915.

Akagi, T., A. Ikegami, T. Tsujimoto, S. Kobayashi, A. Sato, A. Kono and K. Yonemori. 2009b. DkMyb4 is a Myb transcription factor involved in proanthocyanidin biosynthesis in persimmon fruit. Plant Physiol. 151: 2028–2045.

Aron, P. M. and J. A. Kennedy. 2008. Flavan-3-ols; nature, occurrence and biological activity. Mol. Nutri. Food Res. 52: 79–104.

Bogs, J., M. O. Downey, J. S. Harvey, A. R. Ashton, G. J. Tanner and S. P. Robinson. 2005. Proanthocyanidin synthesis and expression of genes encoding leucoanthocyanidin reductase and anthocyanidin reductase in developing grape berries and grapevine leaves. Plant Physiol. 139: 652–663.

Cai, Y., F. J. Evans, M. F. Roberts, J. D. Phillipson, M. H. Zenk and Y. Y. Gleba. 1991. Polyphenolic compounds from Croton lechleri. Phytochemistry 30: 2033–2040.

Cos, P., T. De Bruyne, N. Hermans, S. Apers, D. V. Berghe and A. J. Vlietinck. 2004. Proanthocyanidins in health care: current and new trends. Curr. Med. Chem. 11: 1345–1359.

Davis, A. L., Y. Cai, A. P. Davies and J. R. Lewis. 1996. ^{1}H and ^{13}C NMR assignments of some green tea polyphenols. Magn. Resonance Chem. 34: 887–890.

Dixon, R. A., D-Y. Xie and S. B. Sharma. 2005. Proanthocyanidins—a final frontier in flavonoid research? New Phytol. 165: 9–28.

Downey, M. O., J. S. Harvey and S. P. Robinson. 2003. Analysis of tannins in seeds and skins of Shiraz grapes throughout berry development. Aust. J. Grape Wine Res. 9: 15–27.

Hashimoto, F., G. Nonaka and I. Nishioka. 1989. Tannins and related compounds. XC. 8-*C*-ascorbyl (−)-epigallocatechin 3-*O*-gallate and novel dimeric flavan-3-ols, oolonghomobisflavans A and B, from oolong tea. Chem. Pharm. Bull. 37: 3255–3263.

Ikeda, I., M. Yamada, A. Kurihara and T. Nishida. 1985. Inheritance of astringency in Japanese persimmon. J. Japan. Soc. Hort. Sci. 54: 39–45 (In Japanese with English abstract).

Ikegami, A., A. Kitajima and K. Yonemori. 2005. Inhibition of flavonoid biosynthetic gene expression coincides with loss of astringency in pollination-constant, non-astringent (PCNA)-type persimmon fruit. J. Hort. Sci. Biotech. 80: 225–228.

Kennedy, J. A. and G. P. Jones. 2001. Analysis of proanthocyanidin cleavage products following acid-catalysis in the presence of excess phloroglucinol. J. Agric. Food Chem. 49: 1740–1746.

Lepiniec, L., I. Debeaujon, J. M. Routaboul, A. Baudry, L. Pourcel, N. Nesi and M. Caboche. 2006. Genetics and biochemistry of seed flavonids. Annu. Rev. Plant Biol. 57: 405–430.

Matsuo, T. and S. Ito. 1978. The chemical structure of kaki-tannin from immature fruit of the persimmon (*Diospyros kaki* L.). Agric. Biol. Chem. 42: 1637–1643.

McMahon, L. R., T. A. McAllister, B. P. Berg, W. Majak, S. N. Acharya, J. D. Popp, B. E. Coulman, Y. Wang and K. J. Cheng. 2000. A review of the effects of forage condensed tannins on ruminal fermentation and bloat in grazing cattle. Can. J. Plant Sci. 80: 469–485.

Merghem, R. M., M. Jay, N. Brun and B. Voirin. 2004. Qualitative analysis and HPLC isolation and identification of proanthocyanidins from *Vicia faba*. Phytochem. Anal. 15: 95–99.

Nakagawa, T., A. Nakatsuka, K. Yano, S. Yasugahira, R. Nakamura, N. Sun, A. Itai, T. Suzuki and H. Itamura. 2008. Expressed sequence tags from persimmon at different development stages. Plant Cell Rep. 27: 931–938.

Nakatsubo, F., K. Enokita, K. Murakami, K. Yonemori, A. Sugiura, N. Utsunomiya and S. Subhadrabandhu. 2002. Chemical structures of the condensed tannins in the fruits of *Diospyros* species. J. Wood Sci. 48: 414–418.

Pang, Y., G. J. Peel, E. Wright, Z. Wang and R. A. Dixon. 2007. Early steps in proanthocyanidin biosynthesis in the model legume *Medicago truncatula*. Plant Physiol. 145: 601–615.

Pourcel, L., J. Routaboul, L. Kerhous, M. Caboche, L. Lepiniec and I. Debeaujon. 2005. *TRANSPARENT TESTA 10* encodes a laccase-like enzyme involved in oxidative polymerization of flavonoid in Arabidpsis seed coat. Plant Cell 17: 2966–2980.

Schofield, P., D. M. Mbugua and A. N. Pell. 2001. Analysis of condensed tannins: A review. Animal Feed Sci. Technol. 91: 21–40.

Takos, A. M., B. E. Ubi, S. P. Robinson and A. R. Walker. 2006. Condensed tannin biosynthesis genes are regulated separately from other flavonoid biosynthesis genes in apple fruit skin. Plant Sci. 170: 487–499.

Tanaka, T., R. Takahashi, I. Kouno and G. Nonaka. 1994. Chemical evidence for de-astringency (insolubilization of tannins) of persimmon fruit. J. Chem. Soc. Perkin Trans. 1: 3013–3022.

Tanner, G. J., K. T. Francki, S. Abrahams, J. M. Watson; P. J. Larkin and A. R. Ashton. 2003. Proanthocyanidin biosynthesis in plants. Purification of legume leucoanthocyanidin reductase and molecular cloning of its cDNA. J. Biol. Chem.

278: 31647–31656.
Winkel-Shirley, B. 2001. Flavonoid biosynthesis. A colorful model for genetics, biochemistry, cell biology, and biotechnology. Plant Physiol. 126: 485–493.
Xie, D-Y. and R. A. Dixon. 2005. Proanthocyanidin biosynthesis—still more questions than answers? Phytochemistry 66: 2127–2144.
Xie, D-Y., S. B. Sharma and R. A. Dixon. 2004. Anthocyanidin reductases from *Medicago truncatula* and *Arabidopsis thaliana*. Arch. Biochem. Biophys. 422: 91–102.
Xie, D-Y., S. B. Sharma, N. L. Paiva, D. Ferreira and R. A. Dixon. 2003. Role of anthocyanidin reductase, encoded by BANYULS in plant flavonoid biosynthesis. Science 299: 396–399.
Yonemori, K., A. Sugiura and M. Yamada. 2000. Persimmon genetics and breeding. Plant Breed. Rev. 19: 191–225.

Holzforschung, Vol. 64, pp. 61–67, 2010 • Copyright © by Walter de Gruyter • Berlin • New York. DOI 10.1515/HF.2010.015

Cellular distribution of coniferin in differentiating xylem of *Chamaecyparis obtusa* as revealed by Raman microscopy

Yohei Morikawa[1], Arata Yoshinaga[1,*], Hiroshi Kamitakahara[2], Munehisa Wada[1] and Keiji Takabe[1]

[1] Laboratory of Tree Cell Biology, Division of Forest and Biomaterials Science, Graduate School of Agriculture, Kyoto University, Kyoto, Japan

[2] Laboratory of the Chemistry of Biomaterials, Division of Forest and Biomaterials Science, Graduate School of Agriculture, Kyoto University, Kyoto, Japan

*Corresponding author.
Laboratory of Tree Cell Biology, Division of Forest and Biomaterials Science, Graduate School of Agriculture, Kyoto University, Kitashirakawa-Oiwake-cho, Sakyo-ku, Kyoto 606-8502, Japan
Phone: +81-75-753-6241
Fax: +81-75-753-6302
E-mail: aryosshy@kais.kyoto-u.ac.jp

Abstract

Cellular distribution of coniferin in differentiating xylem of Japanese cypress (*Chamaecyparis obtusa*) was analyzed by Raman microscopy. Small blocks were collected from differentiating xylem, frozen, cut on their surface with a sliding microtome, and then freeze-dried. Scanning electron microscopy showed numerous needle-like deposits in the tracheid lumina from the beginning of the S_1 layer formation to the S_2 layer-forming stage. The Raman spectrum of the deposits in the tracheid lumen was similar to that of coniferin. The presence of coniferin in a water extract from differentiating xylem was confirmed by matrix-assisted laser desorption/ionization time-of-flight mass spectroscopy and ^{1}H- and ^{13}C-nuclear magnetic resonance spectra. Differential Raman spectra taken from samples before and after washing with water and dehydration in an ethanol showed that developing secondary walls contained coniferin during the S_2 layer-forming stage and also after S_3 layer formation. In contrast, coniferin was detected in the cell corner middle lamella during the S_2 layer-forming stage, and the differential spectra were different from that of coniferin after S_3 layer formation. The differential spectrum in this stage was similar to that of a dehydrogenation polymer of coniferyl alcohol prepared by the "zulauf" method (bulk polymerization). These results suggest that free lignin oligomers of the type bulk polymerizate might exist in the cell corner middle lamella during the S_3 layer-forming stage and can be removed from specimens during washing and dehydration. The results can be interpreted in a way that no such oligomer exists in the secondary wall during the same stage owing to endwise addition of monolignols (in analogy to a "zutropf" polymerization).

Keywords: cell wall; *Chamaecyparis obtusa*; coniferin; lignification; matrix-assisted laser desorption/ionization time-of-flight mass spectrometry (MALDI-TOF MS); Raman microscopy; scanning electron microscopy.

Introduction

Lignin is formed by dehydrogenation (radical) polymerization of monolignols (*p*-coumaryl, coniferyl, and sinapyl alcohols) in the presence of hydrogen peroxide and peroxidase. Lignification allows tree cell walls to become more hydrophobic and more decay-resistant against microorganisms, and, in general, to become a composite biopolymer with improved mechanical properties, particularly provided with higher pressure resistance. The lignification process of softwood tracheid cell walls has been studied using various techniques including ultraviolet (UV) microscopy, fluorescence microscopy, microautoradiography, and transmission electron microscopy (Wardrop 1957; Kutscha and Schwarzmann 1975; Imagawa et al. 1976; Takabe et al. 1981a,b, 1985, 1986). Lignification can be divided into three stages: (1) lignification of the cell corner middle lamella and primary walls during S_1 layer formation, (2) slow lignification of the primary walls and the outer part of the secondary walls during S_2 and S_3 layer formation, and (3) very active lignification throughout the secondary walls after S_3 layer formation. Because most of the analytic techniques applied are based on chemical fixation and dehydration through an ethanol series during specimen preparation, the cellular distribution of monolignols removed during preparation is unclear. The monolignol glucoside (coniferin) has long been considered as a participant in lignification (Freudenberg and Harkin 1963; Freudenberg and Torres-Serres 1967; Terazawa et al. 1984). The lignification process in softwood cell walls has also been studied by microautoradiography based on incorporated radiolabeled monolignol glucosides (*p*-glucocoumaryl alcohol, coniferin, and syringin) to differentiating xylem (Terashima and Fukushima 1988; Fukushima and Terashima 1991). It can be concluded that these monolignol glucosides contribute to lignification *in vivo*. Coniferin has been detected in the cambial sap of *Picea excelsa* Link (Freudenberg and Harkin 1963) and in that of six other gymnosperm species (Terazawa et al. 1984). Fukushima et al. (1997) examined coniferin distribution in serial tangential sections prepared from differentiating xylem of 2-year-old shoots of *Pinus thunbergii* and showed that most of the coniferin existed in the cambial zone during the early stages of differentiation.

Coniferyl alcohol glucosyltransferase is an enzyme associated with coniferin biosynthesis from coniferyl alcohol under participation of uridine diphosphate glucose. This enzyme was detected in hypocotyls from 10-day-old spruce [*Picea abies* (L.) Karst.] seedlings by an immunofluorescent technique (Schmid et al. 1982). It was isolated from the cambial zone of *Pinus strobes* (Steeve et al. 2001). Savidge and Forster (1998) analyzed the seasonal activity of this enzyme in the cambial zone and differentiating xylem of *Pinus banksiana* Lamb.

Coniferin-β-glucosidase, an enzyme that hydrolyzes coniferin to coniferyl alcohol and glucose, has been isolated from seedlings of *Picea abies* (Marcinowski et al. 1979) and the seeds of *Glycine max* (Hösel and Todenhagen 1980). Dharmawardhana et al. (1995) also isolated it from differentiating xylem of Lodgepole pine (*Pinus contorta* var *latifolia* Engelm.) and showed that it specifically hydrolyzes coniferin to produce coniferyl alcohol and demonstrated its activity in the cell walls of differentiating xylem. They suggested that coniferin might be transported to the cell wall, where it is hydrolyzed by coniferin-β-glucosidase to coniferyl alcohol. Marjamaa et al. (2003) reported that β-glucosidase activity was highest in May and confirmed the participation of this enzyme on lignification. β-Glucosidase could be localized in tracheid secondary walls of Lodgepole pine by immunoelectron microscopy (Samuels et al. 2002). Accordingly, the involvement of coniferin in lignification is well demonstrated, but the transportation mechanism of monolignols (or monolignol glucosides) remains unclear. Clarification of the cellular distribution of monolignols or monolignol glucosides could contribute to this open question.

Raman microscopy was used to study lignin and cellulose distribution in the cell wall with high resolution (Agarwal 2006; Gierlinger and Schwanninger 2006; Lehringer et al. 2008). The potential of this technique was reviewed by Gierlinger and Schwanninger (2007). Because this technique can be combined with confocal optics, it is not necessary to prepare thin sections (i.e., perform chemical fixation and dehydration to embed samples), as is the case for other techniques such as UV microscopy. This technique can also be used to detect plant flavonoids (Baranska et al. 2006). Therefore, this method is suitable to detect monolignol or monolignol glucosides in lignifying cells. In the present study, we clarified the cellular distribution of coniferin during the lignification process in differentiating xylem of Japanese cypress (*Chamaecyparis obtusa*) by Raman microscopy. The presence of coniferin was also confirmed by matrix-assisted laser desorption/ionization time-of-flight mass spectrometry (MALDI-TOF MS) and nuclear magnetic resonance (NMR) spectroscopy.

Materials and methods

Plant materials

A 22-year-old *Chamaecyparis obtusa* tree grown at the Kitashirakawa Experimental Station, Field Science Education and Research Center, Kyoto University, Kyoto, Japan, was cut on 17 June during active xylem formation. The tree was 11.95 m high with a diameter at breast height of 13.1 cm. Small blocks – 5 mm (rad.)×5 mm (long.)×1 mm (tang.) – containing inner phloem, cambial zone, differentiating xylem, and mature xylem were collected from wood disks. These blocks were frozen and stored at -30°C before the investigation. Small sticks (5 mm×50 mm×1 mm, rad., long., tang., respectively) were also collected from the same location and stored at -30°C to analyze the chemical components removed by washing and dehydration.

Sample preparation for Raman microscopy

The small blocks stored at -30°C were fixed at -20°C with a small drop of water on a cooling plate (Electro Freeze MA-101, KELK Ltd., Hiratsuka, Japan) equipped with a sliding microtome (Yamato Koki Ltd., Asaka, Japan). Transverse sections (50 μm thick) were cut from the blocks. The blocks were removed from the cooling plate, immediately frozen with liquid nitrogen, and freeze-dried with a freeze dryer (FDU-830, Tokyo Rikakikai Co. Ltd., Tokyo, Japan).

Polarizing light microscopy

To confirm the stages of cell wall formation, the sections cut from the surface (as described in the previous section) were dehydrated through an ethanol series and embedded in epoxy resin. Transverse sections (2 μm thick) were cut from the embedded sections and observed under a polarizing microscope with particular focus on the cell wall layers (S_1 and S_3 layers).

Synthesis of the dehydrogenation polymer

Two types of dehydrogenation polymer (DHP) were prepared to record Raman spectra. Endwise polymerization of coniferyl alcohol was performed according to the method of Umezawa and Higuchi (1989). Bulk polymerization of coniferyl alcohol was performed according to the method of Lai and Sarkanen (1975).

Raman microscopy

The Raman microprobe spectrometer was from LabRam HR 350V, Horiba Jobin Yvon, Kyoto, Japan. The spectrometer was equipped with a confocal microscope (Olympus BX40) and an air-cooled charge-coupled device detector (Andor Technology, Belfast, Northern Ireland). The laser excitation wavelength was 633 nm, and an Olympus 50X MPlan objective (N.A. 0.75) was used. Confocal aperture was 800 μm. LabSpec 4.18 software was used to measure the Raman spectrum in the range of 900–1800 cm^{-1}, with baseline correction. After spectra were taken from the surface of the freeze-dried samples, the same samples were washed with water, dehydrated through an ethanol series, and air-dried. Then, spectra were collected again from the same positions. Baseline correction was performed at wave numbers 900, 980, 1205, 1430, 1500, 1560, 1715, and 1800 cm^{-1}. After normalization with an intensity of 1095 cm^{-1} (stretching of polysaccharides), differential spectra were calculated by subtracting the spectra of washed and dehydrated samples from those of freeze-dried samples at the same positions. The cells in differentiating xylem were numbered from the cell that maintained its cell shape to the mature cell closest to the annual ring boundary. The first cell (no. 1) was approximately the second or third cell after the beginning of S_1 layer formation. Spectra were taken from deposits in tracheid lumina, secondary walls, and the cell corner middle lamella of a series of developing tracheids in differentiating xylem.

Scanning electron microscopy

Surfaces of some of the freeze-dried samples and the washed and dehydrated samples were coated with gold using an ion sputtering apparatus (JEE-1100E, JEOL Ltd., Akishima, Japan) and were observed with a scanning electron microscope (JSM-6060, JEOL Ltd., Akishima, Japan) at a 5 kV accelerating voltage.

MALDI-TOF MS and ^{1}H- and ^{13}C-NMR of water extracts from differentiating xylem

Small wood sticks, as described above, were used to collect substances removed during the chemical fixation and dehydration steps for microscopy. Outer and inner bark from the sticks were removed by hand and then cut into small blocks (5 mm length) with a razor blade. These blocks, containing differentiating xylem, were soaked in water overnight. Then, the blocks and their fragments were removed by filtration, and the filtrate was lyophilized. MALDI-TOF MS spectra of the extracts were recorded with a Bruker Reflex III spectrometer in the positive ion and reflector mode. The matrix was 2,5-dihydroxybenzoic acid (DHB) dissolved in methanol/water (1:4, v/v). Some of the blocks containing differentiating xylem were pressed on the target after the inner bark was removed and maintained at room temperature. The residue transferred to the target was also analyzed, as were coniferin, syringin, and *p*-glucocoumaryl alcohol levels. Some of the samples were measured without matrix.

Water extracts (11 mg) were dissolved in 0.5 ml methanol-d_4, and ^{1}H- and ^{13}C-NMR spectra were measured with a Varian INOVA300 FT-NMR spectrometer. The chemical shifts were referenced to tetramethylsilane.

Results and discussion

Coniferin distribution in the cell lumina during lignification

The formation process of cell wall layers, namely S_1, S_2, and S_3 layers, in differentiating xylem was confirmed by polarizing light microscopy. The S_3 layer formed from the 28th cell. Scanning electron microscopy of the freeze-dried sample surfaces showed that there were a relatively large number of needle-like deposits in the tracheid lumina from the beginning of S_1 layer formation to the S_2 layer-forming stage. Figure 1 shows scanning electron micrographs of the lumina of the 19th and 20th tracheids before (Figure 1a) and after (Figure 1b) washing and dehydration. When a small amount of authentic coniferin was observed at the same magnification, its shape also included needle-like deposits (Figure 1c). The shape of the deposit in the lumen of the tracheid during S_2 layer formation was similar to that of coniferin. The Raman spectrum of the needle-like deposit in the lumen of the tracheid observed during S_2 layer formation (Figure 2a) was also similar to that of coniferin (Figure 2b) but different from that of coniferyl alcohol (Figure 2c). These results show that a relatively large amount of coniferin was distributed in the lumen of the S_2 layer forming the tracheids and became a needle-like crystal during freeze-drying.

The presence of coniferin was also confirmed by MALDI-TOF MS and NMR spectroscopy of water extracts from differentiating xylem. Figure 3a shows the MALDI-TOF MS

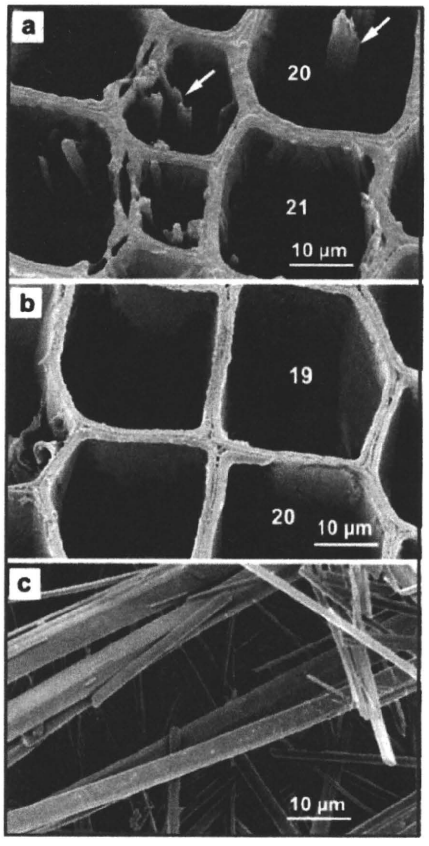

Figure 1 Scanning electron micrographs before (a) and after (b) washing and dehydration of the surfaces of differentiating xylem of *Chamaecyparis obtusa* during S_2 layer formation, and of coniferin (c). Numbers and arrows indicate cell numbers and needle-like deposits in the lumina of tracheids.

spectra of coniferin with DHB as a matrix. Interestingly, coniferin, syringin, and *p*-glucocoumaryl alcohol produced two typical peaks corresponding to an $[M+Na]^+$ and $[M+K]^+$ peak without matrix (Figure 3b–d). These results indicate that these monolignol glucosides themselves might act as a matrix because their chemical structures are similar to sinapic acid, which is commonly used as a matrix for protein investigations by MALDI-TOF MS. Figure 3e shows the spectrum of water extract taken from differentiating xylem without matrix. There were two peaks similar to coniferin ($m/z=365$ and 385). In some experiments, the differentiating xylem stored at -30°C was pressed onto a target after removing the inner bark and was kept at room temperature, and then the sap was transferred to the target. This residue spectrum from the surface of the differentiating xylem in the early stage also showed similar peaks to the water extract (Figure 3f), although the proportion of $[M+K]^+$ was higher than $[M+Na]^+$. Nevertheless, this finding is an indication that the differentiating xylem contained a substance with the same molecular weight as coniferin. Accordingly, this technique can be used to examine the distribution of monolignol glucosides even without matrix.

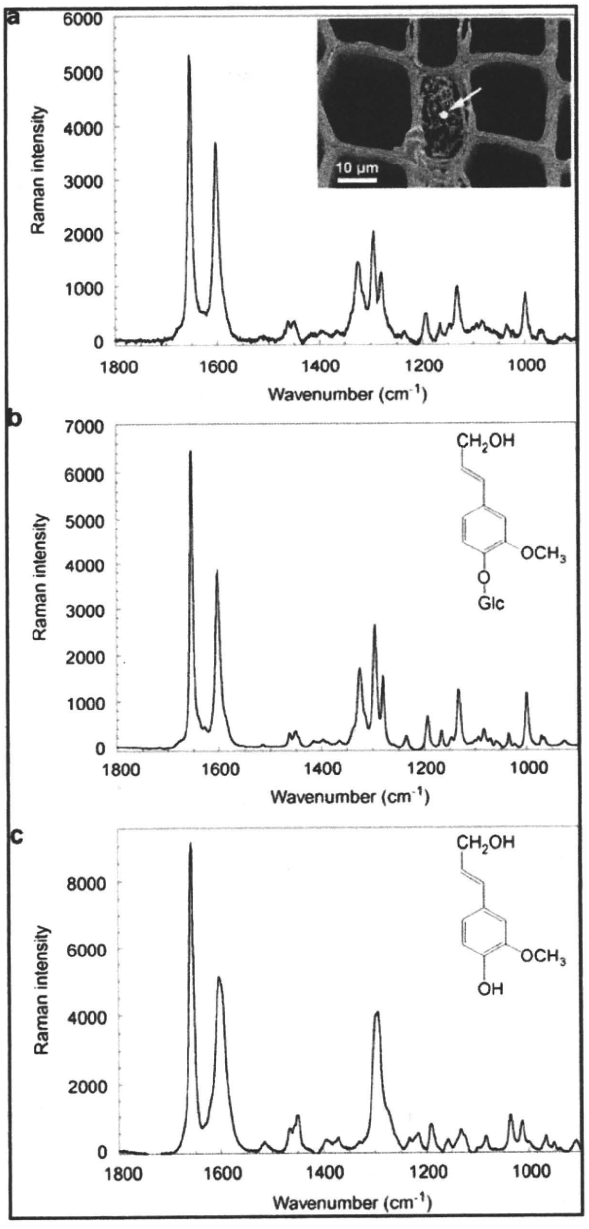

Figure 2 Raman spectra from the needle-like deposits in the lumen (a), coniferin (b), and coniferyl alcohol (c). The spectrum (a) was taken from the position indicated by the white circle in the small scanning electron micrograph.

Figure 4 shows the coniferin ^{1}H-NMR spectra (Figure 4a) and those of the differentiating xylem water extracts (Figure 4b). Analysis of spectra taken by the gCOSY and TOCSY method, compared to a reference (Terashima et al. 1995), confirmed that the extract from differentiating xylem contained coniferin. Figure 4 also presents the coniferin ^{13}C-NMR spectrum (Figure 4c) and that of the water extract (Figure 4d). These spectra also confirmed that the differentiating xylem contains coniferin.

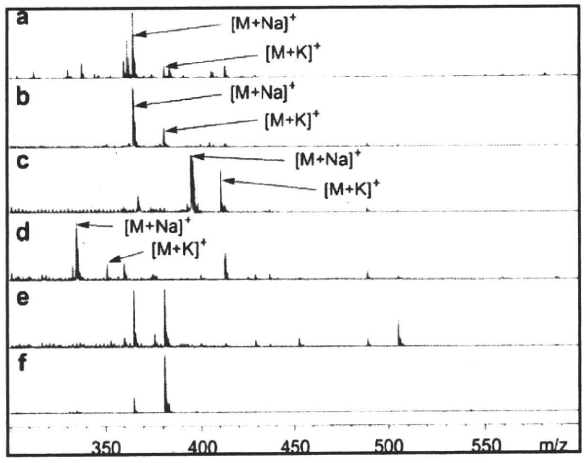

Figure 3 MALDI-TOF MS spectra of coniferin with DHB as the matrix substance (a), coniferin (b), syringin (c), *p*-glucocoumaryl alcohol (d), the water extract from differentiating xylem (e), and the sap residue from differentiating xylem without matrix (f).

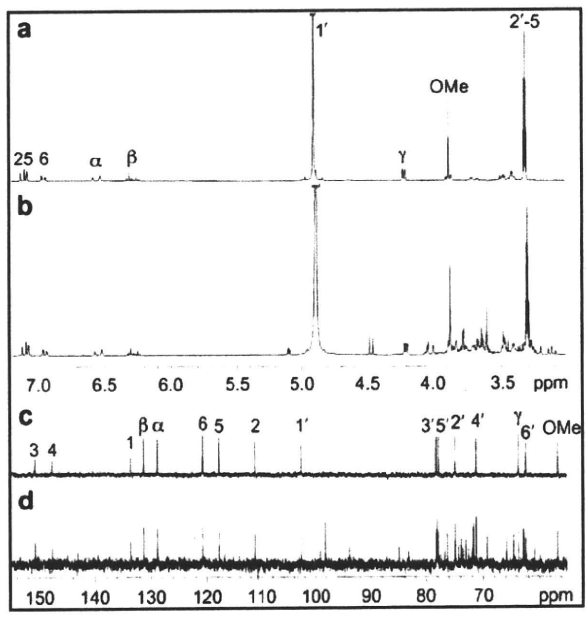

Figure 4 ^{1}H-NMR spectrum of coniferin (a), water extract (b), ^{13}C-NMR spectrum of coniferin (c), and water extract (d). Proton and carbon peaks were assigned based on data of Terashima et al. (1995).

Coniferin distribution in secondary walls during lignification

Raman spectra were taken from the S_1 layer-forming cells to the mature cells to examine coniferin distribution in developing secondary walls. The measurements were performed on two radial files. The Raman intensity at 1600 cm^{-1} (C=C in aromatic ring) and at 1660 cm^{-1} (C=C in side chain) was plotted versus the cell number (Figure 5a). Although there was cell-to-cell variation, the intensities at 1600 cm^{-1} and

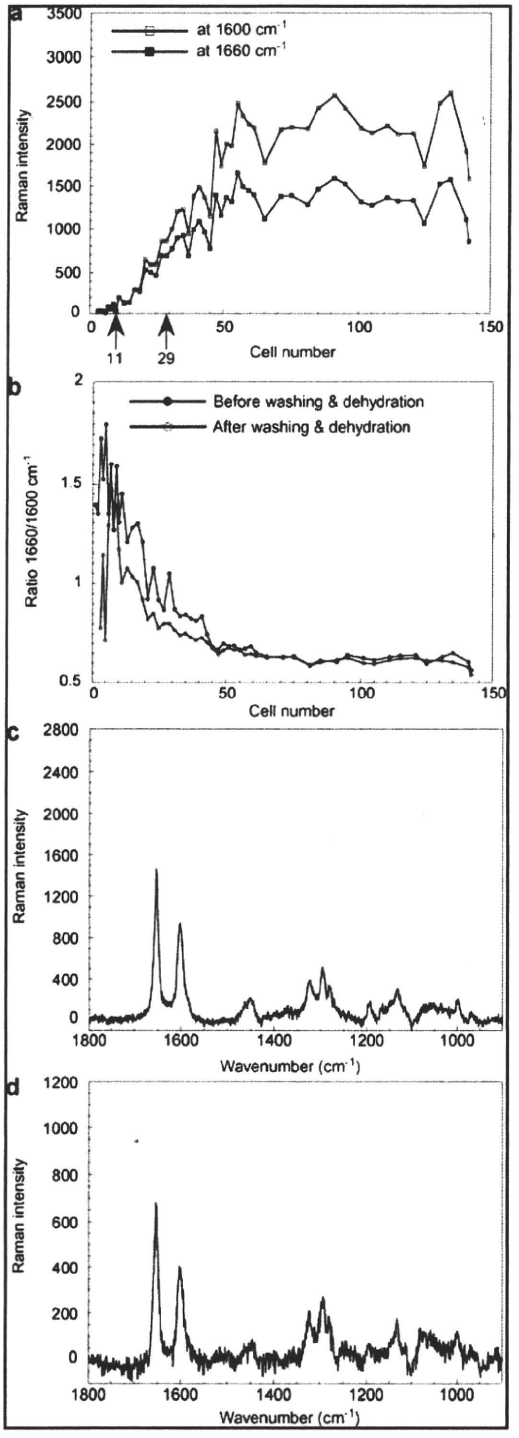

Figure 5 Change in Raman intensity at 1600 cm^{-1} (open square) and 1660 cm^{-1} (closed square) after washing and dehydration (a), intensity ratio of 1660/1600 before (closed circle) and after (open circle) washing and dehydration during lignification of the tracheid secondary walls (b), and the differential spectra before and after washing and dehydration of the tracheid secondary wall during S_2 layer formation (c, cell number 11) and after S_3 layer formation (d, cell number 29).

1660 cm^{-1} increased and then became almost constant at a high level. This observation is due to an increase in lignin content in the developing cell walls. Figure 5b shows the ratio of 1660 cm^{-1}/1600 cm^{-1} before and after washing and dehydration. The intensity ratio 1660/1600 after washing and dehydration is higher during the early stage of cell wall formation and then decreases and becomes constant around the 50th cell. This ratio reflects the proportion of C=C double bonds in the side chain of the polymerized lignin. It is obvious that the proportion of C=C double bonds is higher during the early stage of lignification and decreases and becomes constant at a low level in later stages of lignification. The ratio before washing and dehydration is higher in the S_2 layer-forming stage. It is also true for cells shortly after their S_3 layers were formed. This difference in intensity ratios before and after washing can be interpreted as the presence of coniferin or coniferyl alcohol in the secondary walls during this stage, particularly because the ratios of spectra of both coniferin and coniferyl alcohol are also much higher (Figure 2b,c) than those of the lignified cell wall. Figure 5c,d shows differential spectra from secondary walls before and after washing and dehydration at the S_2 layer-forming stage (cell number no. 11, Figure 5c) and just after S_3 layer formation (cell number no. 29, Figure 5d). Interestingly, these differential spectra were similar to the coniferin spectrum (Figure 2b). These results indicate that coniferin was present in the secondary walls during the S_2 layer-forming stage and the short time after S_3 layer formation.

Coniferin distribution in the cell corner middle lamella during lignification

Figure 6 shows the Raman intensities at 1600 cm^{-1} and 1660 cm^{-1} (Figure 6a) and the intensity ratios of the bands at 1660 cm^{-1}/1600 cm^{-1} (Figure 6b) from the cell corner middle lamella during lignification. The measurements were performed on three radial files. Similar to the secondary walls (Figure 5), the intensities at both wave numbers and their ratios increase in the early stage and then become constant soon after S_3 layer formation. These results also indicate that the proportion of C=C double bonds is higher in the early stage of lignification and then decreases and becomes constant at a low level in later stages of lignification. Before washing and dehydration, the ratio was higher before the S_3 layer formation. The differential spectrum taken in the S_2 layer-forming stage (Figure 6c) was similar to that of coniferin, whereas the spectrum recorded after S_3 layer formation (Figure 6d) was different from the spectrum of coniferin. The differential spectrum was more similar to that of a bulk polymerized DHP (Figure 7a) rather than that of an endwise polymerized DHP (Figure 7b). This finding might be as a result of the presence of free lignin oligomers in the cell corner middle lamella after S_3 layer formation, which can be removed by washing and dehydration. There was no difference in the secondary wall spectra after S_3 layer formation. Our interpretation is that the secondary wall lignin is formed by the endwise polymerization mode with slow addition of monolignols, in the course of which large molecules are syn-

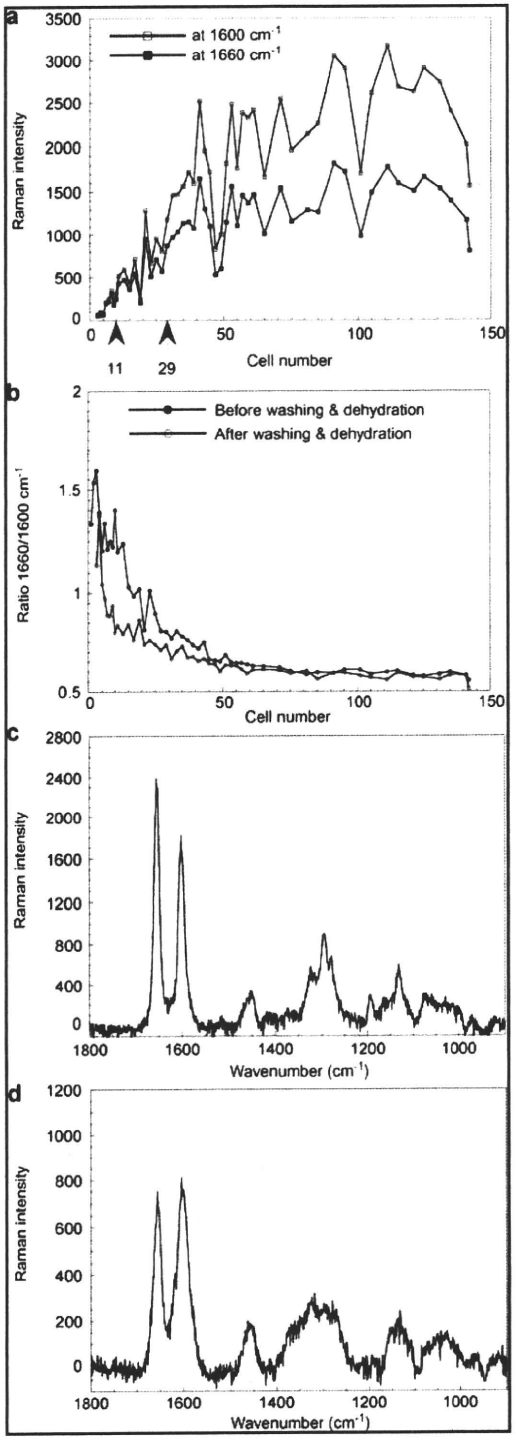

Figure 6 Change in Raman intensity at 1600 cm^{-1} (open square) and 1660 cm^{-1} (closed square) after washing and dehydration (a), intensity ratio of 1660/1600 before (closed circle) and after (open circle) washing and dehydration during lignification of the tracheid cell corner middle lamella (b), and differential spectra before and after washing and dehydration of the tracheid cell corner middle lamella during S_2 layer formation (c, cell number 11) and after S_3 layer formation (d, cell number 29).

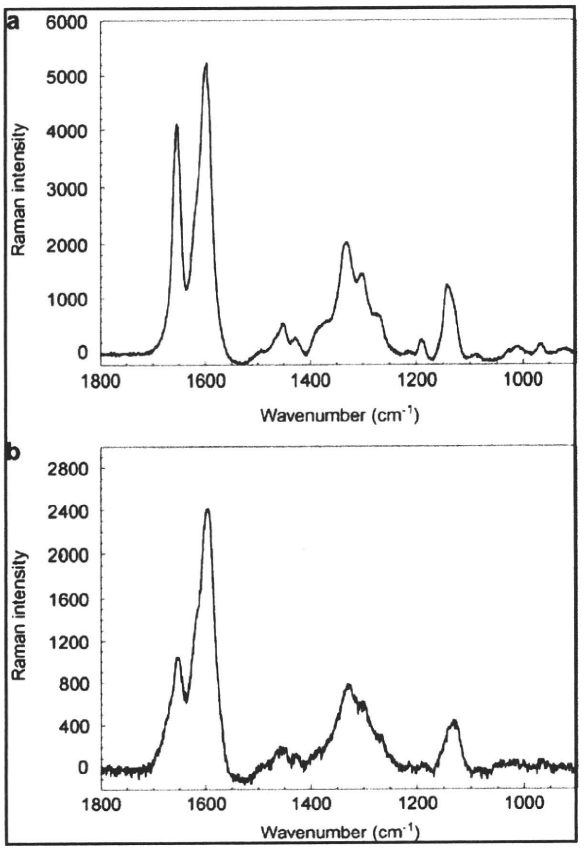

Figure 7 Raman spectra from bulk polymerized DHP (a), and endwise polymerized DHP (b).

thesized, so that free oligomers cannot be formed, which can be dissolved by simple extraction.

Conclusion

Raman microscopy revealed that coniferin is present in the lumina of tracheids during S_2 layer formation. Coniferin was also shown to be distributed in the cell corner middle lamella and secondary walls during this stage, whereas bulk polymerized lignin oligomers existed in the cell corner middle lamella after S_3 layer formation. In contrast, coniferin was also distributed in the secondary walls after S_3 layer formation. These results are in agreement with literature data that the secondary wall lignin is formed by the endwise addition of monolignols without previous formation of free oligomers. MALDI-TOF MS and NMR spectra also indicated the presence of coniferin. Coniferin and other monolignol glucosides could be analyzed without matrix, allowing the analysis of the distribution of these monolignol glucosides in wood sections, although spatial resolution of this method is lower than Raman microscopy. The mechanism by which the monolignol glucosides including coniferin are transported from the lumina to the different cell wall layers remains unclear. Future studies that combine techniques such as

Raman microscopy and MALDI-TOF MS without matrix will help clarify the cellular distribution of coniferin and other monolignol glucosides in the differentiating xylem of other tree species.

Acknowledgements

The authors are indebted to Professor Emeritus Noritsugu Terashima, Nagoya University, Japan, for kindly donating *p*-glucocoumaryl alcohol, coniferin, and syringin.

References

Agarwal, U.P. (2006) Raman imaging to investigate ultrastructure and composition of plant cell walls: distribution of lignin and cellulose in black spruce wood (*Picea mariana*). Planta 224:1141–1153.

Baranska, M., Schulz, H., Joubert, E., Manley, M. (2006) In situ flavonoid analysis by FT-Raman spectroscopy: identification, distribution, and quantification of aspalathin in green rooibos (*Aspalathus linearis*). Anal. Chem. 78:7716–7721.

Dharmawardhana, D.P., Ellis, B.E., Carlson, J.E. (1995) A beta-glucosidase from lodgepole pine xylem specific for the lignin precursor coniferin. Plant Physiol. 107:331–339.

Freudenberg, K., Harkin, J.M. (1963) The glucosides of cambial sap of spruce. Phytochemistry 2:189–193.

Freudenberg, K., Torres-Serres, J. (1967) Umvandlung des Phenylalanins in Lignin-bildend Glucoside. Ann. Chem. 703:225–230.

Fukushima, K., Terashima, N. (1991) Heterogeneity in formation of lignin. Part XV: formation and structure of lignin in compression wood of *Pinus thunbergii* studied by microautoradiography. Wood Sci. Technol. 25:371–381.

Fukushima, K., Taguchi, S., Matsui, N., Yasuda, S. (1997) Distribution and seasonal changes of monolignol glucosides in *Pinus thunbergii*. Mokuzai Gakkaishi 43:254–259.

Gierlinger, N., Schwanninger, M. (2006) Chemical imaging of poplar wood cell walls by confocal Raman microscopy. Plant Physiol. 140:1246–1254.

Gierlinger, N., Schwanninger, M. (2007) The potential of Raman microscopy and Raman imaging in plant research. Spectroscopy 21:69–89.

Hösel, W., Todenhagen, R. (1980) Characterization of a beta-glucosidase from *Glycine max* which hydrolyses coniferin and syringin. Phytochemistry 19:1349–1353.

Imagawa, H., Fukazawa, K., Ishida, S. (1976) Study on the lignification in tracheids of Japanese larch, *Larix leptolepis* GORD. Res. Bull. Coll. Exp. Forests Hokkaido Univ. 33:127–138 (in Japanese).

Kutscha, N.P., Schwarzmann, J.M. (1975) The lignification sequence in normal wood of balsam fir (*Abies balsamea*). Holzforschung 29:79–84.

Lai, Y.Z., Sarkanen, K.V. (1975) Structural variation in dehydrogenation polymers of coniferyl alcohol. Cellulose Chem. Technol. 9:239–245.

Lehringer, C., Gierlinger, N., Koch, G. (2008) Topochemical investigation on tension wood fibres of *Acer* spp., *Fagus sylvatica* L. and *Quercus robur* L. Holzforschung 62:255–263.

Marcinowski, S., Falk, H., Hammer, D.K., Hoyer, B., Grisebach, H. (1979) Appearance and localization of a beta-glucosidase hydrolyzing coniferin in spruce (*Picea abies*) seedlings. Planta 144:161–165.

Marjamaa, K., Lehtonen, M., Lundell, T., Toikka, M., Saranpää, P., Fagerstedt, K.V. (2003) Developmental lignification and seasonal variation in beta-glucosidase and peroxidase activities in xylem of Scots pine, Norway spruce and silver birch. Tree Physiol. 23:977–986.

Samuels, A.L., Rensing, K.H., Douglas, C.J., Mansfield, S.D., Dharmawardhana, D.P., Ellis, B.E. (2002) Cellular machinery of wood production: differentiation of secondary xylem in *Pinus contorta* var. *latifolia*. Planta 216:72–82.

Savidge, R.A., Forster, H. (1998) Seasonal activity of uridine 5′-diphosphoglucose: coniferyl alcohol glucosyltransferase in relation to cambial growth and dormancy in conifers. Can. J. Bot. 76:486–493.

Schmid, G., Hammer, D.K., Ritterbusch, A., Grisebach, H. (1982) Appearance and immunohistochemical localization of UDP-glucose: coniferyl alcohol glucosyltransferase in spruce (*Picea abies* (L.) Karst.) seedlings. Planta 156:207–212.

Steeve, V., Forster, H., Pommer, U., Savidge, R. (2001) Coniferyl alcohol metabolism in conifers I. Glucosidic turnover of cinnamyl aldehydes by UDPG: coniferyl alcohol glucosyltransferase from pine cambium. Phytochemistry 57:1085–1093.

Takabe, K., Fujita, M., Harada, H., Saiki, H. (1981a) The deposition of cell wall components in differentiating tracheids of Sugi. Mokuzai Gakkaishi 27:249–255 (in Japanese).

Takabe, K., Fujita, M., Harada, H., Saiki, H. (1981b) Lignification process of Japanese black pine (*Pinus thunbergii* Parl.) tracheids. Mokuzai Gakkaishi 27:813–820 (in Japanese).

Takabe, K., Fujita, M., Harada, H., Saiki, H. (1985) Autoradiographic investigation of lignification in the cell walls of Cryptomeria (*Cryptomeria japonica* D. Don). Mokuzai Gakkaishi 31:613–619.

Takabe, K., Fujita, M., Harada, H., Saiki, H. (1986) Lignification process in Cryptomeria (*Cryptomeria japonica* D. Don) tracheid: electron microscopic observation of lignin skeleton of differentiating xylem. Res. Bull. Col. Exp. Forests Hokkaido Univ. 43:783–788.

Terashima, N., Fukushima, K. (1988) Heterogeneity in formation of lignin VI: an autoradiographic study of the heterogeneous formation and structure of pine lignin. Wood Sci. Technol. 22:259–270.

Terashima, N., Ralph, R.A., Landucci, L.L. (1995) New facile syntheses of monolignol glucosides; *p*-glucocoumaryl alcohol, coniferin and syringin. Holzforschung 50:151–155.

Terazawa, M., Okuyama, H., Miyake, M. (1984) Phenolic compounds in living tissues of woods. I. Phenolic beta-glucosides of 4-hydroxycinnamyl alcohol derivatives in the cambial sap of woods. Mokuzai Gakkaishi 30:322–328.

Umezawa, T., Higuchi, T. (1989) Cleavages of aromatic ring and beta-O-4 bond of synthetic lignin (DHP) by lignin peroxidase. FEBS Lett. 242:325–329.

Wardrop, A.B. (1957) The phase of lignification in the differentiation of wood fibers. Tappi 40:225–243.

Received June 22, 2009. Accepted August 14, 2009.
Previously published online December 7, 2009.

Holzforschung, Vol. 64, pp. 173–181, 2010 • Copyright © by Walter de Gruyter • Berlin • New York. DOI 10.1515/HF.2010.026

Studies on the dehydrogenative polymerization of monolignol β-glycosides. Part 6: Monitoring of horseradish peroxidase-catalyzed polymerization of monolignol glycosides by GPC-PDA

Yuki Tobimatsu[1,2], Toshiyuki Takano[1,*], Hiroshi Kamitakahara[1] and Fumiaki Nakatsubo[3]

[1] Division of Forest and Biomaterials Science, Graduate School of Agriculture, Kyoto University, Kyoto, Japan
[2] Department of Biochemistry, University of Wisconsin-Madison, Madison, WI, USA
[3] Research Institute for Sustainable Humanosphere, Kyoto University, Kyoto, Japan

*Corresponding author.
Division of Forest and Biomaterials Science, Graduate School of Agriculture, Kyoto University, Kitashirakawa-oiwakecho Sakyo-ku, Kyoto, 606-8502, Japan
Phone: +81-75-753-6255
Fax: +81-75-753-6300
E-mail: takatmys@kais.kyoto-u.ac.jp

Abstract

Horseradish peroxidase (HRP)-catalyzed dehydrogenative polymerization of guaiacyl (G) and syringyl (S)-type monolignol γ-*O*-glucosides, isoconiferin (iso-G) and isosyringin (iso-S), which contain a hydrophilic glucosyl unit on γ-position of coniferyl alcohol and sinapyl alcohol, respectively, was monitored by gel permeation chromatography coupled with photodiode array detection (GPC-PDA). Contrary to the conventional dehydrogenative polymerization of monolignols, the polymerization of the glycosides produces water-soluble synthetic lignins (DHPs) in a homogeneous aqueous phase. Taking advantage of this unique reaction system, the method was developed to follow the changes of molecular weights in the course of DHP formations. Moreover, PDA detection permits determination of oligomeric S-type quinone methide intermediates (QMs) formed as stable transient compounds during polymerization of iso-S. A detailed comparison of the polymerization profiles revealed entirely different behaviors of G- and S-type monomers. The data strongly support the view that the low reactivity of oligomeric S-type QMs impedes the formation of DHPs from S-type monomers. In copolymerization of G- and S-type monomers, it is conceivable that G-type phenolic hydroxyl groups serve as good nucleophilic reactants to scavenge S-type QMs resulting in efficient production of DHPs. As a consequence, the present approach can be a powerful tool to study the *in vitro* dehydrogenative polymerization providing further mechanistic insights into lignin polymerization *in vivo*.

Keywords: dehydrogenation polymer (DHP); dehydrogenative polymerization; gel permeation chromatography (GPC); horseradish peroxidase (HRP); lignin biosynthesis; monolignol β-D-glucoside; photodiode array (PDA) detection; quinone methide (QM); syringyl lignin.

Introduction

The last stage of lignin biosynthesis in plant tissues is generally defined as a process of the enzymatic dehydrogenative polymerization of monolignols such as coniferyl alcohol (G-alc), sinapyl alcohol (S-alc), and *p*-coumaryl alcohol (H-alc), giving rise to guaiacyl (G), syringyl (S), and *p*-hydroxyphenyl (H) lignins, respectively. It is well established that this polymerization process is easily mimicked *in vitro* by the enzymatic oxidative polymerization of monolignols leading to lignin polymer models (dehydrogenation polymers, DHPs) (Freudenberg 1965). As reviewed by several authors (Brunow et al. 1998; Boerjan et al. 2003; Grabber 2005; Ralph et al. 2004, 2008), this versatile model system has allowed various modifications of the polymerization parameter to be studied *in vitro* and provided much information on the relationship between the reaction environment and the resulting lignin structures in relation to lignin polymerization *in vivo*.

However, the chemical structures of DHPs are generally different from those of native lignins (Terashima et al. 1995, 1996; Saake et al. 1996; Landucci et al. 1998). For example, DHPs are well reported to contain relatively small amounts of the β-O-4 interunit linkage, whereas that linkage is the most predominant and accounts for more than half among the various interunit linkages in native lignins. It is also reported that typical DHPs have lower molecular weights than those of isolated lignins such as milled wood lignins (MWL) (Higuchi et al. 1971; Faix et al. 1981; Tanahashi et al. 1982; Cathala et al. 2003). Although many factors affecting the in vitro dehydrogenative polymerization have been raised, a satisfactory synthesis of DHPs resembling native lignins is still challenging. This emphasizes the need for a better understanding of the dehydrogenative polymerization process.

Several authors investigated the time-course of the oxidative polymerization of monolignols or their analogs using HPLC (Terashima and Atalla 1995; Aoyama et al. 2002; Sasaki et al. 2004), GC (Kobayashi et al. 2005), capillary zone electrophoresis (Fournand and Lapierre 2001; Fournand

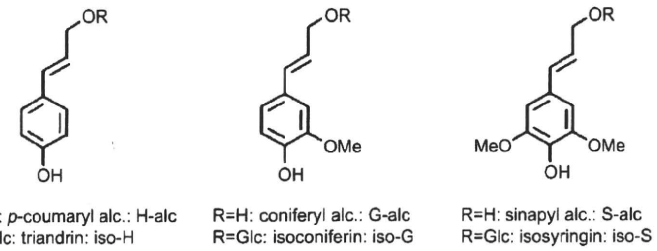

Figure 1 Chemical structures of monolignols and monlignol glycosides.

et al. 2003), UV spectroscopy (Sterjiades et al. 1993; Takahama et al. 1996; Kobayashi et al. 2005; Hatfield et al. 2008) or matrix-assisted laser desorption/ionization time-of-flight mass spectrometry (De Angelis et al. 1996). However, current analytical data are generally on the chemistry of the products obtained in the initial stage of polymerization such as monomer conversions or oligomerization reactions. There are few reports in which the whole process of the dehydrogenative polymerization of monolignols was monitored.

Recently, we investigated the enzymatic dehydrogenative polymerization of monolignol γ-*O*-glucosides [triandrin (iso-H); isoconiferin (iso-G); isosyringin (iso-S) (Figure 1)], which contain D-glucosyl units on the γ-positions of monolignols (Tobimatsu et al. 2006, 2008a,b). Owing to the presence of highly hydrophilic sugar units attached to monolignols, the polymerization of the glycosides produces water-soluble DHPs in a homogeneous aqueous phase, whereas the conventional polymerization of monolignols yields water-insoluble DHPs in a heterogeneous reaction system.

Data in our previous studies reveal that this unique model system based on the glycosides would be a powerful tool to monitor DHP formation. Moreover, information about the whole chemistry in the course of the homogeneous polymerization mixtures can be obtained by techniques of solution-state spectroscopy or liquid chromatography. In our previous report, UV spectroscopy was applied for the real-time monitoring of the HRP-catalyzed polymerization of the glycosides (Tobimatsu et al. 2008c). Importantly, our approach established the unexpectedly stable presence of S-type quinone methide intermediates (QMs, Figure 2) during the polymerization of S-type glycoside, iso-S, whereas no such stable intermediates were detectable during the polymerization of G-type glycoside, iso-G. It has been recognized that the preparations of high molecular weight DHPs from S-type monolignol and analogs are difficult (Freudenberg and Hübner 1952; Yamasaki et al. 1976; Higuchi et al. 1977; Faix and Besold 1978; Sterjiades et al. 1993; Weymouth et al. 1993; Yoshida et al. 1994, 1998; Aoyama et al. 2002; Kobayashi et al. 2005; Tobimatsu et al. 2008a). Data in our previous study demonstrate that the low reactivity of S-type QMs possibly impedes the formation of DHP from iso-S as well as from S-alc (Tobimatsu et al. 2008c).

In the present study, gel permeation chromatography coupled with photodiode array detection (GPC-PDA) is applied to monitor the HRP-catalyzed polymerization and copolymerization of G- and S-type glycosides, i.e., iso-G and iso-S. GPC techniques are suitable to reveal the progressive changes of molecular masses of oligomer and polymer type intermediates during polymerization. Simultaneously, the PDA detection offers the UV absorption patterns of the polymerization products, providing additional information about the structural changes during polymerization. The polymerization behaviors of iso-G and iso-S will be discussed in terms of the polymerization efficiency and the reactivity of QMs as key intermediates.

Materials and methods

The monolignol glycosides, iso-G and iso-S were synthesized as previously reported (Takano et al. 2006). HRP (100 U mg^{-1}) was purchased from Wako Pure Chemical Co. (Osaka, Japan) and used without further purification. Other chemicals were purchased from Nacalai Tesque Inc. (Kyoto, Japan) or Wako Pure Chemical Co. and used as received.

GPC-PDA monitoring of HRP-catalyzed dehydrogenative polymerization

The HRP-catalyzed polymerization of iso-G or iso-S was carried out as follows. Three solutions were prepared. Solution A: 2 mg of HRP in 500 μl of 0.05 M phosphate buffer (pH 6.5); solution B: 20 μmol of monomer in 2500 μl of the buffer; solution C: 2500 μl of hydrogen peroxide (24 μmol) aqueous solution. Solutions B and

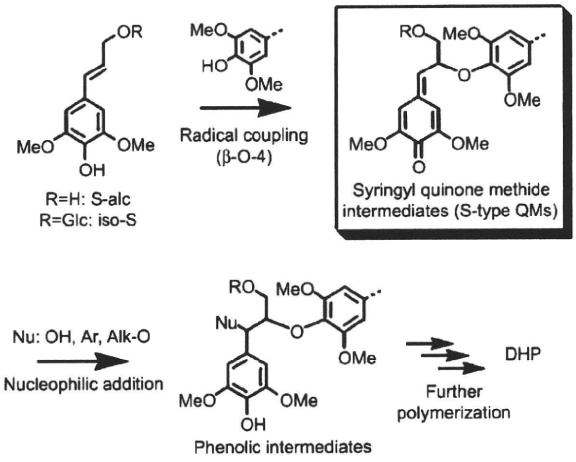

Figure 2 Syringyl quinone methide intermediates (S-type QMs) formed in the dehydrogenative polymerization of the γ-O-glycoside of sinapyl alcohol (iso-S) or sinapyl alcohol (S-alc).

C were simultaneously pumped to solution A at a constant rate of 1.25, 2.5, or 15 ml h^{-1} (monomer addition time: 10, 60 or 120 min). Reaction mixtures (100 μl) were sequentially sampled, immediately mixed with 900 μl of 0.1 M LiCl in *N,N*-dimethylformamide (DMF), cooled at 0°C and subjected to the GPC-PDA analyses within 15 min after withdrawing from the reaction mixtures.

The HRP-catalyzed copolymerization of iso-G and iso-S was carried out in the same manner as described above, except the compositions in solutions B and C. The mixture of iso-G and iso-S (iso-G/iso-S = 2/20, 5/20, 10/20, 15/20 μmol) in 2500 μl of 0.05 M phosphate buffer (pH 6.5) was used for solution B. For solution C, a hydrogen peroxide (1.2 eq. mol for total monomers in solution B) in 2500 μl water was prepared. The addition rate of solutions B and C to solution A was set to 2.5 ml h^{-1} (monomer addition time: 60 min).

The GPC-PDA analyses were performed on a Shimadzu LC-20A LC system (Shimadzu, Japan) equipped with a photodiode array detector (SPD-M20A; Shimadzu). Elution conditions: column TSK gel α-M (Tosoh, Japan); eluent 0.1 M LiCl in DMF; flow rate 0.5 ml min^{-1}; column oven temperature 40°C; injection volume 20 μl. Conditions for PDA detection: cell temperature 40°C; scan region 260–400 nm; band width 4 nm; response 1280 ms. Molecular weight calibration is based on polystyrene standards (Shodex, Japan). The data acquisition and computation was done with LC-solution version 1.22 SP1 software (Shimadzu). Before injection, sample solutions were filtered through a 0.45 μm PTFE disposable membrane (Advantec, Japan).

Stability of S-type QMs from iso-S in the GPC-PDA monitoring

For quantitative determination of S-type QMs formed in the HRP-catalyzed polymerization of iso-S, the stability of S-type QMs in the GPC-PDA monitoring was investigated. The solution (3 ml) consisting of 20 μM iso-S and 2 mg of HRP in 50 mM sodium phosphate buffer (pH 6.5) was kept at 25°C under stirring. The polymerization was initiated by adding 30 μl of a 0.816% hydrogen peroxide aqueous solution (24 μM) to the mixture. After 10 min reaction time, 100 μl of the reaction mixture containing S-type QMs was sampled, mixed with 900 μl of 0.1 M LiCl in DMF and stored at 0°C under identical conditions as described above for polymerization monitoring. At a given storage time after sampling (5, 15, 30, 45, 60 min), 20 μl of the solution was injected into the GPC-PDA system. Three runs for each storage time were carried out. A loss of S-type QMs during the storage was evaluated by the decrease in the GPC peak area detected at 344 nm. A quasi-linear decrease in the peak from S-type QMs with the storage time was observed. The peak area at storage time of 0 was obtained from extrapolation and the proportions of remaining S-type QMs are plotted against the storage time in Figure 3. As a result, the loss of S-type QMs at 15 min storage time was estimated to be 0.4% (the standard deviations were around 2%). This confirms that S-type QMs were semi-quantitatively determined by the presented monitoring experiments because the sample storage time in the monitoring experiments was within 15 min, as described above.

Results and discussion

GPC-PDA monitoring of the polymerization of iso-G

Dehydrogenative polymerization of iso-G initiated by HRP was carried out under similar conditions as described previously for the syntheses of DHPs (Tobimatsu et al. 2006). Aqueous solutions of the monomer and hydrogen peroxide were added simultaneously to a buffer (pH 6.5, 25°C) containing HRP. At a given reaction time, an aliquot of the homogeneous reaction mixtures was sampled and subjected to GPC-PDA. It was preliminary confirmed that isolated DHPs from the glycosides are completely soluble in the DMF eluent in the range of concentrations used in the present work. Therefore, it can be stated that whole polymerization mixtures were accessible in the GPC-PDA analyses.

Figure 4a shows GPC-PDA profiles of iso-G polymerization (monomer addition rate: 2.5 ml h^{-1}). In the profile at the reaction time of 0 min, the strong absorptions from iso-G at 272 and 300 nm are visible, whereas the absorption maximums were observed at 274 nm in the profiles at the reaction time of 30 and 180 min (Figure 4a2). As shown in the GPC profiles, the elution peaks shifted to higher molar mass regions as reaction time progressed, indicating the growth of DHP chains (Figure 4a3). In Figure 5, the weight- and number-average molecular weights (M_w and M_n) – calculated based on the elution chromatograms at 274 nm detection – are plotted against the polymerization time for DHPs with different monomer addition rates. In all the reactions, the values of M_w and M_n increased rapidly at the initial stage of the polymerization and further increased gradually at later stages. The slow addition of the monomer solution increases the molecular masses. These results support the well-known and generally accepted facts that molecular masses of DHPs prepared by the "end-wise" polymerization methods (slow addition of monomers) are higher than those of DHPs prepared by the "bulk" polymerization method (simultaneous reaction of all reactants) (Sarkanen 1971; Cathala et al. 1998; Tobimatsu et al. 2006). The results of GPC-PDA monitoring of iso-G polymerization confirm that polymerization proceeds without formation of stable (low molecular) intermediates.

GPC-PDA monitoring of the polymerization of iso-S

HRP-catalyzed polymerization of iso-S was conducted under identical reaction conditions to those described for iso-G monomers. However, the polymerization profiles of iso-S

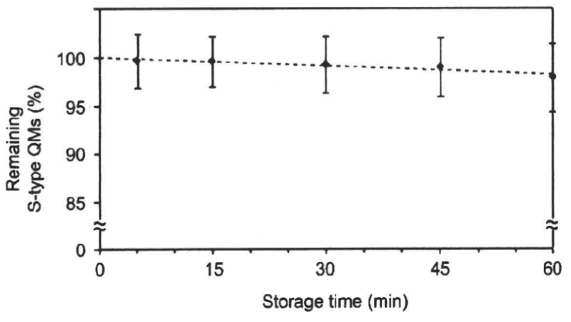

Figure 3 Remaining amounts of S-type QMs over a storage time after sampling from the HRP-catalyzed polymerization mixtures from iso-S determined by GPC-PDA. (For abbreviations see Figures 1 and 2.)

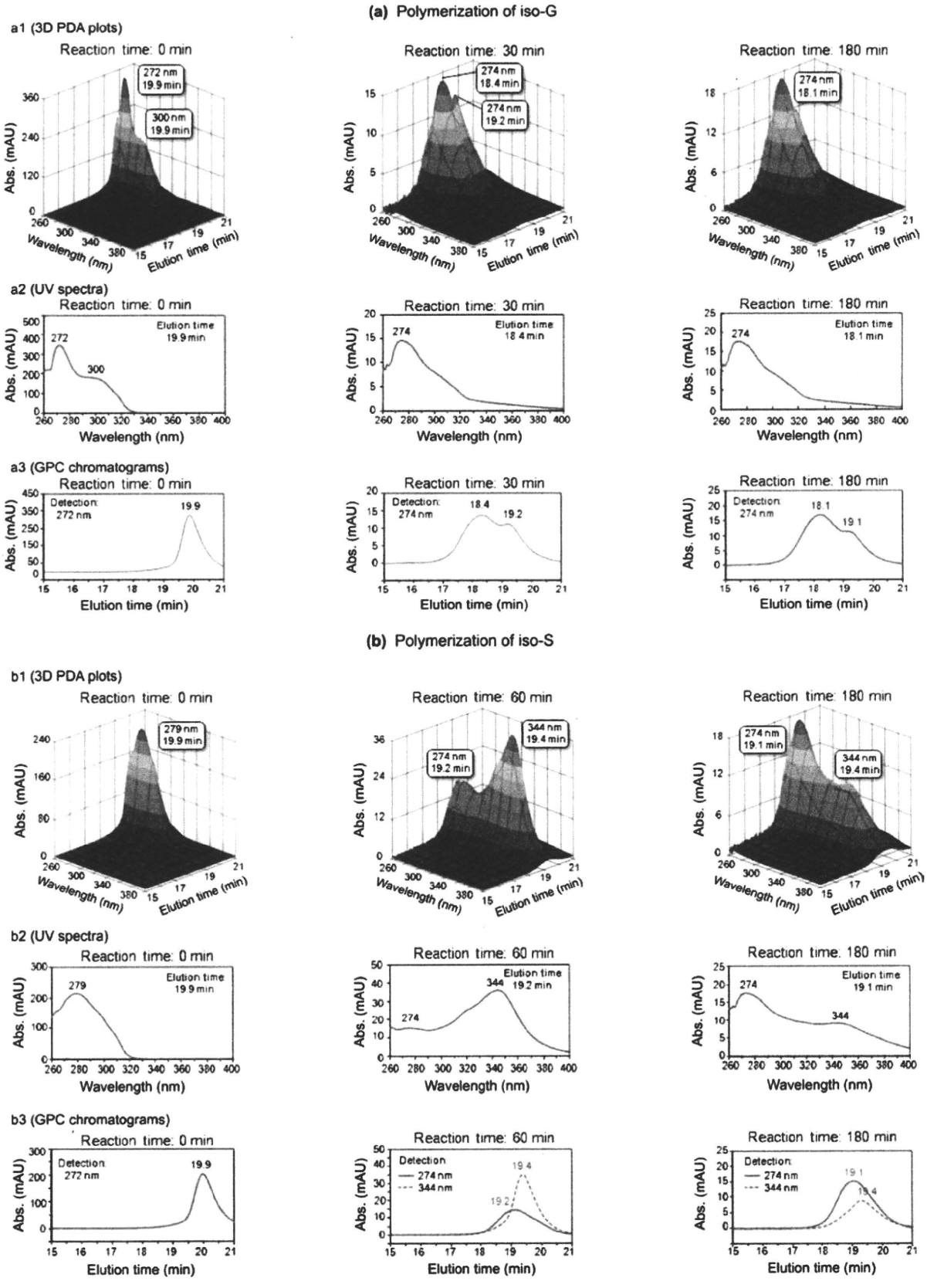
(a) Polymerization of iso-G
a1 (3D PDA plots)
Reaction time: 0 min
272 nm 19.9 min
300 nm 19.9 min
Reaction time: 30 min
274 nm 18.4 min
274 nm 19.2 min
Reaction time: 180 min
274 nm 18.1 min
Abs. (mAU)
Wavelength (nm)
Elution time (min)
a2 (UV spectra)
Reaction time: 0 min
Elution time 19.9 min
272
300
Reaction time: 30 min
Elution time 18.4 min
274
Reaction time: 180 min
Elution time 18.1 min
274
Wavelength (nm)
a3 (GPC chromatograms)
Reaction time: 0 min
Detection: 272 nm
19.9
Reaction time: 30 min
Detection: 274 nm
18.4
19.2
Reaction time: 180 min
Detection: 274 nm
18.1
19.1
Elution time (min)
(b) Polymerization of iso-S
b1 (3D PDA plots)
Reaction time: 0 min
279 nm 19.9 min
Reaction time: 60 min
344 nm 19.4 min
274 nm 19.2 min
Reaction time: 180 min
274 nm 19.1 min
344 nm 19.4 min
b2 (UV spectra)
Reaction time: 0 min
Elution time 19.9 min
279
Reaction time: 60 min
Elution time 19.2 min
344
274
Reaction time: 180 min
Elution time 19.1 min
274
344
b3 (GPC chromatograms)
Reaction time: 0 min
Detection: 272 nm
19.9
Reaction time: 60 min
Detection
274 nm
344 nm
19.4
19.2
Reaction time: 180 min
Detection
274 nm
344 nm
19.1
19.4

(Figure 4 continued)

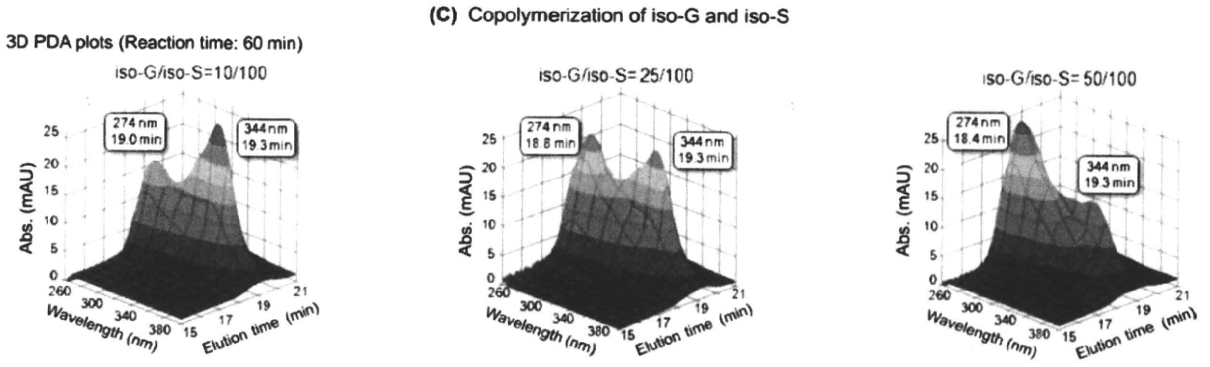

Figure 4 GPC-PDA profiles of HRP-catalyzed polymerization of iso-G (a), iso-S (b), and copolymerization of iso-G and iso-S (c). Monomer addition rate: 2.5 ml h^{-1}. The reaction time 0 is defined as the time at which the monomer addition was started.

(Figure 4b) are different from those of iso-G, a finding which confirms the observation made in our previous studies. As shown by the UV spectra at the elution maximums (Figure 4b2), the absorptions from iso-S at 279 nm disappear after initiating the polymerization, indicating a complete conversion of iso-S into other compounds. The formation of phenolic intermediates can be followed by absorptions at 274 nm and characteristic temporary absorptions at 344 nm from relatively stable S-type QMs are observable, as evidenced in our previous study (Tobimatsu et al. 2008c). The GPC measurements permit the determination of the phenolic intermediates and S-type QMs separately, based on the maxima at 274 nm and 344 nm, respectively (Figure 4b3). The calculated molecular weights of the products formed are plotted against the reaction time in Figure 6. As reaction time progressed, the molecular weights of phenolic intermediates (274 nm detection) increased, but these data are much lower than those observed in iso-G polymerization experiments (Figure 6a). The monomer addition rate, at least in the range investigated, shows little effect on the growth of polyphenolic chains in the polymerization of iso-S. The molecular weights calculated based on 344 nm detection were even lower than those of phenolic intermediates based on 274 nm detection and remained almost constant around $M_n = 1200$, which is corresponding to degree of polymerization (DP) = ca. 3 (Figure 6b). This clearly indicates that oligomeric S-type QMs with less reactivity accumulate significantly during iso-S polymerization. The accumulation of these products can be determined by the quantitative evaluations of GPC chromatograms detected at 344 nm (Figure 7). Preliminary experiments demonstrated that the loss of S-type QMs after sampling is negligibly small (0.4%) under the present analytical conditions (Figure 3). Accordingly, the S-type QMs reached a maximum shortly after the reaction started and decreased very slowly as reaction time progressed. Although slow addition of the monomer solution suppressed accumulation of S-type QMs at the initial stage of polymerization, still high levels of S-type QMs accumulations were observed in all polymerization experiments with iso-S.

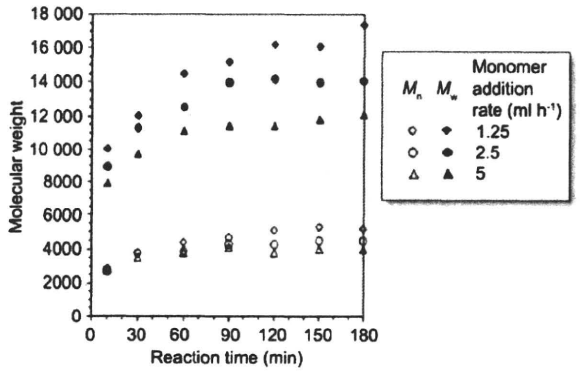

Figure 5 Product molecular weights calculated based on GPC chromatograms detected at 274 nm during the course of HRP-catalyzed polymerization of iso-G. M_w, weight average molecular weight. M_n, number average molecular weight.

These findings support the results in our previous studies (Tobimatsu et al. 2008c). The low reactivity of S-type QMs can be explained by reduced positive charge density at the α-positions owing to the presence of two electron-donating methoxyl groups, and can also be related to the steric hindrance for the formation of syringyl α-O-4 structures. It is reported that the analogous quinone methide, 2,6-di-*tert*-butyl-4-methylene-2,5-cyclohexadienone reacts very slowly in aqueous media. Bolton et al. (1990, 1992) pointed out that this low reactivity is as a result of the lack of hydrogen bonding between the shielded oxo group and water molecules, suppressing charge separation of the quinone methide. The same is true for the low reactivity of S-type QMs during the dehydrogenative polymerization. Recently, a production of DHP with high yield was observed in HRP-catalyzed polymerization of sinapyl alcohol in the presence of strongly nucleophilic azide ion, which serves as a QM scavenger (Tobimatsu et al. 2008d, 2010). The findings of the present paper can be readily rationalized by the low reactivity of the S-type QMs, which considerably impedes the subsequent polymerizations to DHP.